Claudin-2 suppresses GEF-H1, RHOA, and MRTF, thereby impacting proliferation and profibrotic phenotype of tubular cells

Received for publication, November 10, 2018, and in revised form, August 21, 2019 Published, Papers in Press, September 3, 2019, DOI 10.1074/jbc.RA118.006484

Qinghong Dan[1‡], Yixuan Shi[1‡], Razieh Rabani[‡], Shruthi Venugopal[‡], Jenny Xiao[‡], Shaista Anwer[‡], Mei Ding[‡], Pam Speight[‡], Wanling Pan[§], R. Todd Alexander[§], András Kapus[‡¶], and Katalin Szászi[‡¶2]

From the [‡]Keenan Research Centre for Biomedical Science at St. Michael's Hospital and the [¶]Department of Surgery, University of Toronto, Ontario M5B 1T8, Canada and the [§]Departments of Pediatrics and Physiology, University of Alberta, Edmonton, Alberta T6G 2R3, Canada

Edited by Eric R. Fearon

The tight junctional pore-forming protein claudin-2 (CLDN-2) mediates paracellular Na^+ and water transport in leaky epithelia and alters cancer cell proliferation. Previously, we reported that tumor necrosis factor-α time-dependently alters CLDN-2 expression in tubular epithelial cells. Here, we found a similar expression pattern in a mouse kidney injury model (unilateral ureteral obstruction), consisting of an initial increase followed by a drop in CLDN-2 protein expression. CLDN-2 silencing in LLC-PK1 tubular cells induced activation and phosphorylation of guanine nucleotide exchange factor H1 (GEF-H1), leading to Ras homolog family member A (RHOA) activation. Silencing of other claudins had no such effects, and re-expression of an siRNA-resistant CLDN-2 prevented RHOA activation, indicating specific effects of CLDN-2 on RHOA. Moreover, kidneys from CLDN-2 knockout mice had elevated levels of active RHOA. Of note, CLDN-2 silencing reduced LLC-PK1 cell proliferation and elevated expression of cyclin-dependent kinase inhibitor P27 (P27KIP1) in a GEF-H1/RHOA-dependent manner. P27KIP1 silencing abrogated the effects of CLDN-2 depletion on proliferation. CLDN-2 loss also activated myocardin-related transcription factor (MRTF), a fibrogenic RHOA effector, and elevated expression of connective tissue growth factor and smooth muscle actin. Finally, CLDN-2 down-regulation contributed to RHOA activation and smooth muscle actin expression induced by prolonged tumor necrosis factor-α treatment, because they were mitigated by re-expression of CLDN-2. Our results indicate that CLDN-2 suppresses GEF-H1/RHOA. CLDN-2 down-regulation, for example, by inflammation, can reduce proliferation and promote MRTF activation through RHOA. These findings suggest that the initial CLDN-2 elevation might aid epithelial regeneration, and CLDN-2 loss could contribute to fibrotic reprogramming.

Epithelial layers generate a barrier and mediate controlled transport via transcellular and paracellular pathways. The multiprotein junctional complexes connecting individual cells are key for maintaining structural and functional integrity of the layer. Tight junctions (TJ),[3] located apically, generate apicobasal polarity and the selective paracellular pathways (1, 2). The cytoskeleton is a key regulator of TJ dynamics (2, 3). Accordingly, the small GTPase RHOA, a master regulator of the cytoskeleton, plays a central role in TJ remodeling (4). RHOA cycles between inactive (GDP-bound) and active (GTP-bound) states. Its activity is tightly controlled by three classes of regulators: guanine nucleotide exchange factors (GEFs), GTPase-activating proteins, and guanine nucleotide dissociation inhibitors (5). Activation of RHOA is promoted by GEFs, which constitute a large family with >70 members. Interestingly, the state of the TJs also affects RHOA and the cytoskeleton, likely via the binding of RHOA regulators at the TJs. One such protein is the Dbl family guanine nucleotide exchange factor GEF-H1 (ARHGEF2). GEF-H1 binds to the microtubules and to TJ adapter proteins, including cingulin and paracingulin, that control its activity (6–8). In our previous work we showed that GEF-H1 mediated TNFα-induced RHOA activation in epithelial cells (9). Whether the TJs were involved in TNFα-induced GEF-H1 activation, however, remained unknown.

Claudins, a family of 27 small, tetraspan membrane proteins are an integral part of the TJs and are expressed in a tissue-specific manner (10). They bind their counterparts in neighboring cells in homo- and heterotypic interactions and thus seal off the paracellular space. Some claudins generate selective paracellular channels for ions and water (pore-forming claudins),

This work was supported by grants from the Kidney Foundation of Canada (to K. S. and A. K.) and by Canadian Institutes of Health Research Grants PJT-149058 and MOP-142409 (to K. S.), MOP-106625 (to A. K.), and MOP-136891 (to R. T. A.). The authors declare that they have no conflicts of interest with the contents of this article.

[1] These authors contributed equally to this work.

[2] To whom correspondence should be addressed: Keenan Research Centre for Biomedical Science at St. Michael's Hospital, 209 Victoria St., Rm. 622, Toronto, ON M5B 1T8, Canada. Tel.: 416-847-1752; Fax: 416-864-5167; E-mail: katalin.szaszi@unityhealth.to.

[3] The abbreviations used are: TJ; tight junctions; CDKI, cyclin-dependent kinase inhibitor; Cldn or CLDN, claudin; ECIS, electric cell-substrate impedance sensing; EMT, epithelial–mesenchymal transition; GAPDH, glyceraldehyde-3-phosphate dehydrogenase; IL, interleukin; LCM, laser capture microdissection; MLC, myosin light chain; pMLC, phosphorylated MLC; MRTF, myocardin-related transcription factor; TGF, transforming growth factor; ZO, zonula occludens; PCNA, proliferating cell nuclear antigen; PEP, profibrotic epithelial phenotype; PTEN, phosphatase and tensin homolog; UUO, unilateral ureteral obstruction; TNF, tumor necrosis factor; SRF, serum response factor; GEF, guanine nucleotide exchange factor; SGLT, sodium glucose co-transporter; TER, transepithelial resistance; BrdU, bromodeoxyuridine; MDCK, Madin–Darby canine kidney; CTGF, connective tissue growth factor; SMA, smooth muscle actin; NR, nonrelated; RBD, RHOA-binding domain; DAPI, 4′,6′-diamino-2-phenylindole.

and they have unique permeability properties (10). The differential expression profile of claudins is the basis for tissue-specific epithelial permeability. The cytoplasmic tail of claudins binds PDZ domain–containing adapter proteins (11). These adapters generate multiprotein complexes that link claudins to the junctional actomyosin ring, which contributes to dynamic TJ regulation (3). TJs are also important signaling platforms, providing input for diverse functions such as proliferation, migration, and differentiation (4, 11). Many epithelial cancers display altered claudin expression that correlates with prognosis (12), suggesting that claudins might directly affect tumor growth and metastasis. Nevertheless, the exact mechanistic details of such noncanonical functions remain incompletely understood.

Claudin-2 (CLDN-2) is a pore-forming claudin expressed in epithelial layers with high paracellular permeability such as proximal tubules and the intestine (reviewed in Ref. 10). It forms dynamically gated paracellular cation channels (13) that are also permeable to water (14). Studies using CLDN-2 overexpression or silencing in various cell lines substantiated that CLDN-2 elevates Na^+ and water permeability, thereby reducing transepithelial resistance (14–19). The data obtained in claudin-2 knockout mice further support an important role in energy-efficient paracellular salt transport (20–22). The S2 segment of the proximal tubules of CLDN-$2^{-/-}$ mice showed significantly reduced transepithelial reabsorption of Na^+, Cl^-, and water. Higher energy demand of active transcellular Na^+ absorption compensating for lack of CLDN-2–mediated passive paracellular transport resulted in medullary hypoxia and augmented ischemic kidney injury (22). Thus, the transport function of CLDN-2 appears to be crucial for minimizing oxygen consumption in the kidney and thereby protecting it from injury.

In cancer cell lines manipulation of CLDN-2 expression was shown to alter proliferation (23) and migration (24), and CLDN-2 was found to mediate effects of various pro-proliferative stimuli (*e.g.* (25)). CLDN-2 overexpression in lung adenocarcinoma, colorectal, and breast cancer was associated with poor prognosis (26, 27). Thus, it is conceivable that altered CLDN-2 expression plays a direct pathogenic role through effects on cancer growth and metastasis.

In light of these findings, it is noteworthy that CLDN-2 expression is dynamically modulated by a variety of stimuli through several pathways (28). In intestinal cells, cytokines caused significant up-regulation of CLDN-2, likely contributing to permeability increase in inflammatory bowel disease (29). TNFα-induced changes in CLDN-2 abundance were more complex in tubular cells, where an initial increase in CLDN-2 levels caused by reduced degradation was followed by a drop in mRNA and protein expression (19). In cultured tubular cells, a variety of pathologically relevant chronic stimuli were shown to reduce CLDN-2 expression. These include metabolic acidosis (30), hyperosmolarity (31), H_2O_2 (32), and the immunosuppressant drugs sirolimus and cyclosporine A (33). Because CLDN-2 affects proliferation, it is conceivable that its loss may modify recovery from kidney injury. Nevertheless, the consequences of altered tubular CLDN-2 expression beyond transport remain largely undefined.

Considering these gaps in our knowledge, the overall objective of this study was to explore how CLDN-2 expression is affected by kidney injury and to obtain mechanistic insights into downstream consequences of altered tubular CLDN-2 expression. Because TJs can affect RHOA signaling, we explored the effects of CLDN-2 on RHOA. Our data demonstrate that CLDN-2 is a negative regulator of RHOA signaling. Loss of CLDN-2 causes RHOA-dependent decrease in proliferation and promotes fibrogenic epithelial reprogramming. These findings highlight the potential functional significance of cytokine-induced CLDN-2 changes beyond effects on permeability.

Results

CLDN-2 expression is reduced in a mouse model of obstructive nephropathy

We have previously shown that in cultured tubular cells TNFα altered expression of the channel forming TJ protein CLDN-2 in a biphasic manner, with an initial increase followed by a drop (19). However, the effects of kidney injury and inflammation on CLDN-2 expression *in vivo* remained unknown. Therefore, we used unilateral ureteral obstruction (UUO) in mice, as in our earlier studies (34, 35), to evaluate changes in CLDN-2 abundance. UUO is an obstructive nephropathy model, in which the primary trigger for injury is epithelial mechanical stretch caused by elevated intratubular pressure after ureteral ligation (36). Injury causes tubulointerstitial inflammation characterized by the presence of a large array of cytokines. Significant tubulointerstitial fibrosis develops by day 7 (36). As shown in Fig. 1(*A*, see *right panel* for quantitation, and *B*), UUO caused a time-dependent change in the abundance of CLDN-2 protein and mRNA, normalized to tubulin (protein) or GAPDH (mRNA). Initially, CLDN-2 protein and mRNA levels significantly increased (day 3). This was followed by a large drop in CLDN-2 protein by day 7, when fibrosis developed. Interestingly, although the protein dropped significantly below the basal level at day 7, mRNA expression was reduced compared with day 3 but remained around the baseline (sham) level. This suggests that the observed decrease in CLDN-2 protein was likely due to augmented degradation. In contrast to CLDN-2, the mRNA of claudin-1 and 7 showed a substantial and significant increase in UUO at 7 days (Fig. 1*C*).

UUO causes tubular injury, and therefore we wished to exclude the possibility that loss of tubular cells accounts for reduced CLDN-2 levels. Although the lack of change in CLDN-2 mRNA suggests that at this time point proximal tubular cells are viable, to further substantiate this conclusion, we measured mRNA levels of the sodium glucose co-transporter-2 (SGLT-2), that is expressed exclusively in the proximal tubules. We found no difference in SGLT-2 mRNA expression in sham and UUO at any time point (Fig. 1*D*). Finally, we used laser capture microdissection (LCM) as earlier (34, 35) to assess tubular markers. LCM allows the isolation of the tubular compartment, and thus the quantification of mRNA is not confounded by a change in other cell types, *e.g.* by influx of immune cells. As shown in Fig. 1*E*, UUO did not change expression of Na^+/Cl^- co-transporter (NCC), basic amino acid transporter 1

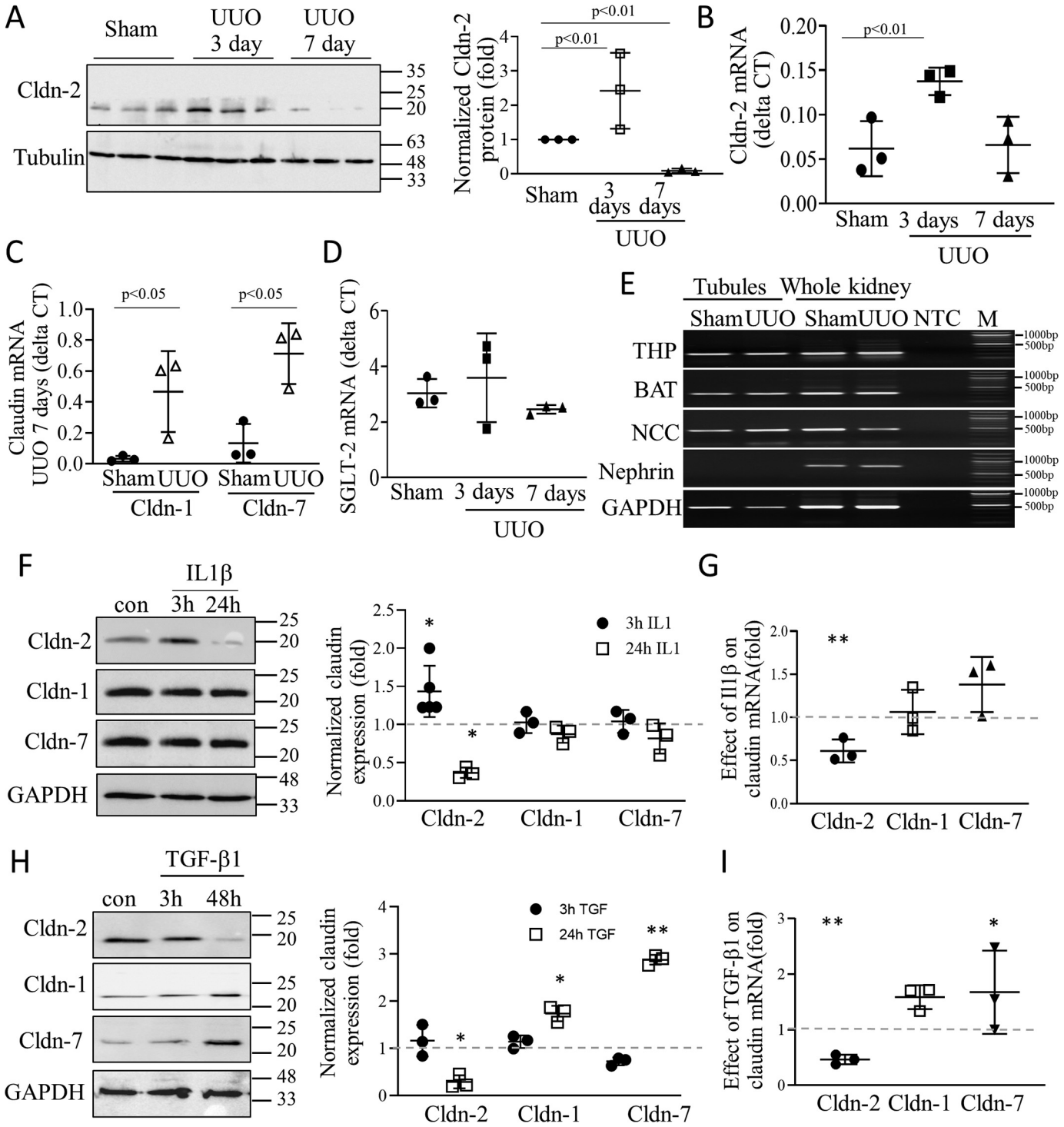

Figure 1. *A–C*, changes in claudin expression in a mouse nephropathy model. *A*, whole kidney lysates were prepared from mice 3 or 7 days after sham or UUO operation and probed for Cldn-2 and tubulin. Three samples/condition are shown from different animals. Cldn-2 expression was normalized to tubulin and expressed as fold change from sham (means ± S.D. $n = 3$). *B–D*. mRNA of Cldn-2, SGLT-2, Cldn-1, Cldn-7, and the housekeeping gene GAPDH were quantified in whole kidney samples from sham or UUO (3 or 7 days, as indicated) using quantitative PCR. Claudin and SGLT-2 mRNA values were normalized to GAPDH (means ± S.D. $n = 3–5$). *E*, UUO does not cause loss of tubules. The mice were subjected to sham or UUO operation, and 7 days later the tubules were isolated using laser capture microdissection. Compartment marker mRNAs were detected using end-point PCR. The tubular markers were: THP, Tamm–Horsfall protein; BAT, basic amino acid transporter; and NCC, Na/Cl co-transporter. *First* and *second lanes*, tubular samples from sham and UUO mice, respectively; *third* and *fourth lanes*, whole kidney samples from sham and UUO mice; *fifth lane*, no template control. *Sixth lane*, molecular weight marker. *F–I*, effect of IL1β and TGFβ1 on Cldn expression in tubular cells. LLC-PK$_1$ cells were grown to confluence and treated with 10 ng/ml IL1β or TGFβ for the indicated times. *F* and *H*, Cldn-1, -2, and -7 and the loading control protein GAPDH were detected by Western blotting and quantified as above. Normalized Cldn levels were expressed as fold from control, set as 1 (means ± S.D., $n = 3–5$). *G* and *I*, LLC-PK$_1$ cells were treated with 10 ng/ml IL1β or TGFβ for 24 h, and mRNA was quantified using quantitative PCR, as above. GAPDH was used for normalization. Fold changes from control. The *dashed line* indicates the control set to 1. Graph shows means ± S.D. ($n = 3$). *, $p < 0.05$; **, $p < 0.01$.

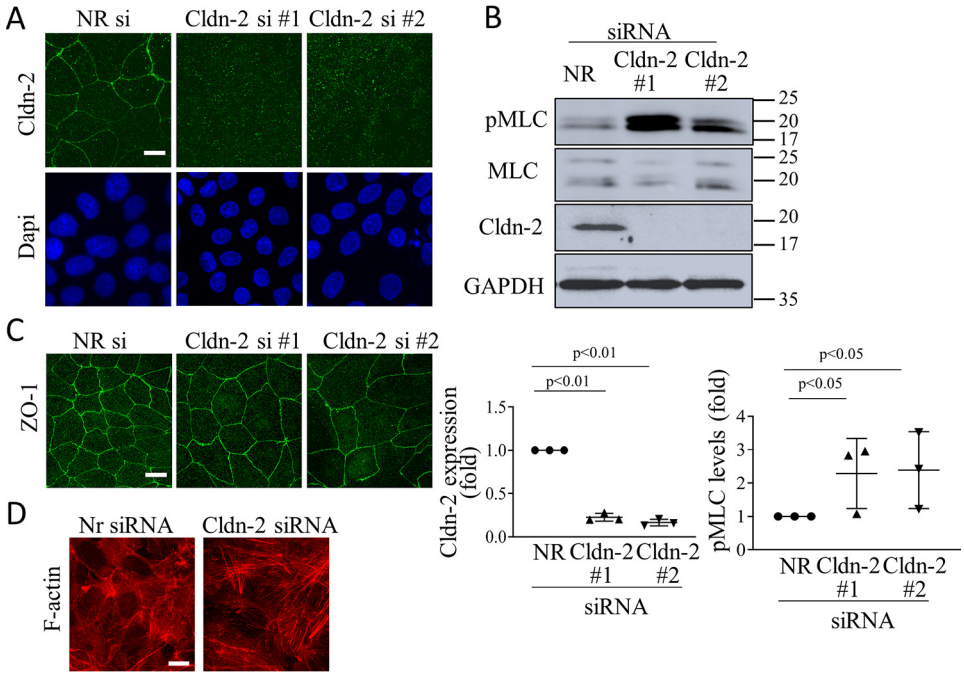

Figure 2. Claudin-2 silencing does not prevent TJ formation but elevates pMLC levels. LLC-PK$_1$ cells were transfected with NR or Cldn-2–specific siRNA #1 or #2 as indicated, and 2 days later either fixed with ice-cold methanol (*A*) or paraformaldehyde (*C* and *D*), or lysed (*B*). In *A*, *C*, and *D*, immunofluorescent staining was performed using antibodies against Cldn-2 (*A*) or ZO-1 (*C*) or phalloidin rhodamine to label F-actin (*D*). In *A*, nuclei were counterstained with DAPI. Z-stacks were obtained using confocal microscopy, and maximal intensity projection pictures were generated using the Metamorph software. In *D*, Z stacks were obtained from the bottom of the cells to visualize stress fibers. The *bar* represents 10 μm. *B*, cells were lysed, and the indicated proteins were detected by Western blotting. Note that two MLC isoforms are visualized by the antibodies. Densitometric analysis shows normalized Cldn-2 and pMLC levels expressed as fold from control (means ± S.D., $n = 3$).

(BAT1), or Tamms–Horsfall protein, markers of various tubular segments. Taken together, CLDN-2 protein changes are specific, and the late reduction is unlikely to be due to a mass loss of proximal tubule cells.

Cytokines play a crucial role in the development of fibrosis, and prolonged exposure to TNFα reduced CLDN-2 expression in tubular cells (19). Therefore, we next tested the effects of other relevant cytokines that are increased in UUO. We exposed LLC-PK$_1$ tubular cells to IL1β and found that short-term (3 h) stimulation caused an increase in CLDN-2 expression but had no effect on Cldn-1 or 7 (Fig. 1*F*). In contrast, in cells exposed to IL1β for 24 h, abundance of CLDN-2 but not the other claudins showed a significant drop. Moreover, this effect was accompanied by a significant drop in CLDN-2 mRNA, suggesting a reduction in synthesis (Fig. 1*G*). This time-dependent biphasic effect is similar to the effects of TNFα we reported earlier (19). Next, we assessed the effect of TGFβ1, the main pro-fibrotic cytokine on claudin expression. As shown on Fig. 1*H*, none of the claudins were affected by short-term TGFβ1 treatment. In contrast, long-term TGFβ1 treatment significantly reduced both CLDN-2 protein and mRNA expression (Fig. 1, *H* and *I*), similarly to IL1β. Interestingly, long-term TGFβ1 treatment significantly elevated Cldn-1 and -7 protein expression (Fig. 1*H*). This was likely due to increased synthesis, because mRNA of these claudins also showed an increase, although the combined effect at this time point did not reach statistical significance for Cldn-1 (Fig. 1*I*). Taken together, these data suggest that inflammatory/fibrogenic cytokines affect expression of various claudins during kidney injury and inflammation. Specifically, CLDN-2 expression changes in a time-dependent manner, and CLDN-2 levels drop in conjunction with the development of renal fibrosis.

Claudin-2 silencing causes actin remodeling and myosin phosphorylation

We next aimed at establishing the consequences of CLDN-2 loss. To this end, we silenced CLDN-2 in LLC-PK$_1$ cells using two different siRNAs, both of which caused >80% reduction in CLDN-2 expression (Fig. 2, *A* and *B*). Because CLDN-2 is an integral part of the TJs, we first wished to establish that CLDN-2 silencing does not disrupt the TJs. In previous studies we have demonstrated that CLDN-2 silencing did not interfere with the establishment of a confluent monolayer and had no effect on claudin-1 peripheral localization (19). In fact, the transepithelial resistance (TER) of the layer was higher following CLDN-2 silencing, reflecting the absence of a main channel forming claudin (19). To further verify that the junctions were preserved following CLDN-2 silencing, we visualized the TJ-associated adapter ZO-1 by immunofluorescence (Fig. 2*C*). No change was observed in ZO-1 localization or expression in cells transfected with CLDN-2 siRNA. The TJs are coupled to the actomyosin belt that plays a key role in their regulation (3). The TJs have also been shown to bind several regulators of small GTPase signaling, thereby affecting cytoskeleton organization (4). Therefore, we next asked whether CLDN-2 silencing alters the actomyosin cytoskeleton. Our data show that CLDN-2 silencing elevated the overall level of phosphorylated myosin light chain (pMLC) (Fig. 2*B*). The antibody against MLC and pMLC visualized a doublet, as in previous studies, correspond-

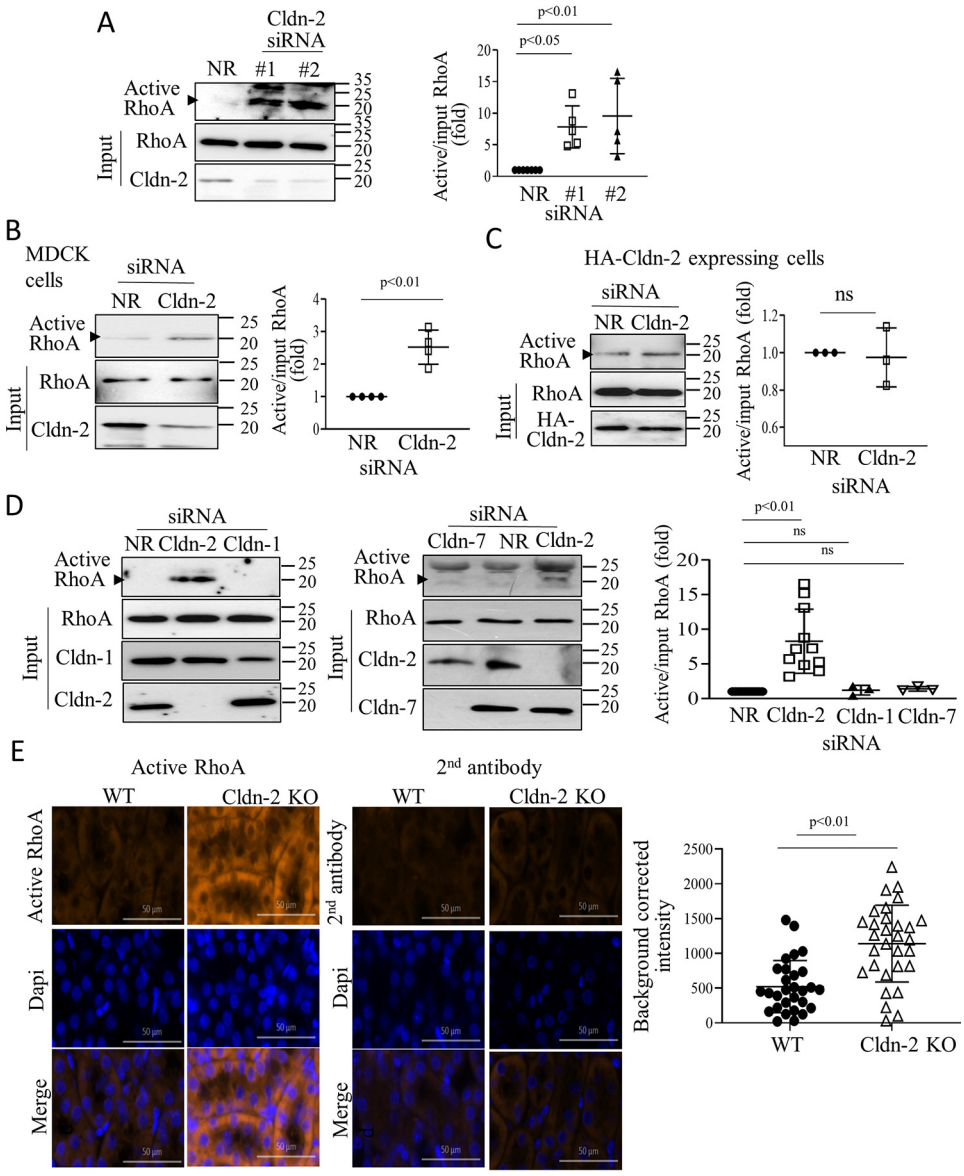

Figure 3. Claudin-2 silencing activates RhoA. *A–D*, WT LLC-PK$_1$ cells (*A* and *D*) or MDCK cells (*B*) or HA-claudin-2 expressing LLC-PK$_1$ cells (*C*) were transfected with NR or Cldn-1, -2, or -7–specific siRNAs, as indicated. 48 h after transfection, the cells were lysed, and active RhoA was captured using GST–RBD-coupled beads. Precipitated and total RhoA were detected by Western blotting. RhoA in the precipitate (active) is indicated by the *arrowhead*. Note that in some blots, the antibody also visualized a nonspecific band above the RhoA-specific band. The identity of the RhoA band was verified by silencing. Active RhoA was normalized to the corresponding input (total) RhoA and in each experiment expressed as fold from NR siRNA transfected control. The indicated claudins were detected in total cell lysates to verify silencing. Graphs show means ± S.E. $n = 3–5$. *E*, active RhoA staining is elevated in Cldn-2 KO mice. Active RhoA was detected in kidney sections obtained from WT or Cldn-2 KO mice using a RhoA-GTP–specific antibody (*left top row*). The *right top row* shows labeling with the secondary antibody alone. *Middle row*, nuclear stain with DAPI; *bottom row*, merged images. *Bar*, 50 μm. Intensity of the labeling was quantified using the Zen software in regions of 100-μm diameter (>30 regions/animals in three KO and two WT animals). Average labeling in samples exposed to the secondary antibody only was subtracted from each intensity value (means ± S.D.)

ing to two isoforms detectable in LLC-PK$_1$ cells (37). Both CLDN-2 siRNAs caused a well-detectable increase in the phosphorylation of both MLC isoforms. Next, we visualized F-actin using fluorescently labeled phalloidin. Whereas the control cells contained fewer and finer stress fibers, in cells transfected with CLDN-2 siRNA stress fibers were thicker and more numerous (Fig. 2*D*). Thus, CLDN-2 silencing did not prevent TJ formation but resulted in alterations in actomyosin.

Loss of claudin-2 causes RHOA activation

Because the small GTPase RHOA is a key regulator of F-actin and pMLC, we next asked whether CLDN-2 silencing affected RHOA activity. We performed a Rhotekin–RHOA-binding domain (RBD) precipitation assay, as previously (38), using lysates of cells transfected with nonrelated (NR) siRNA or two different CLDN-2 siRNAs. As shown on Fig. 3*A*, in cells transfected with CLDN-2 siRNA, significantly more RHOA was precipitated by Rhotekin-RBD, indicating RHOA activation. In many RHOA activation assays, we observed a nonspecific band at ~25 kDa. The identity of the RHOA-specific band at 20 kDa (labeled with an *arrowhead*) was validated using an siRNA (Fig. 4*A*). The two CLDN-2 siRNAs induced similar RHOA activation. To demonstrate that RHOA activation induced by CLDN-2 loss was not a

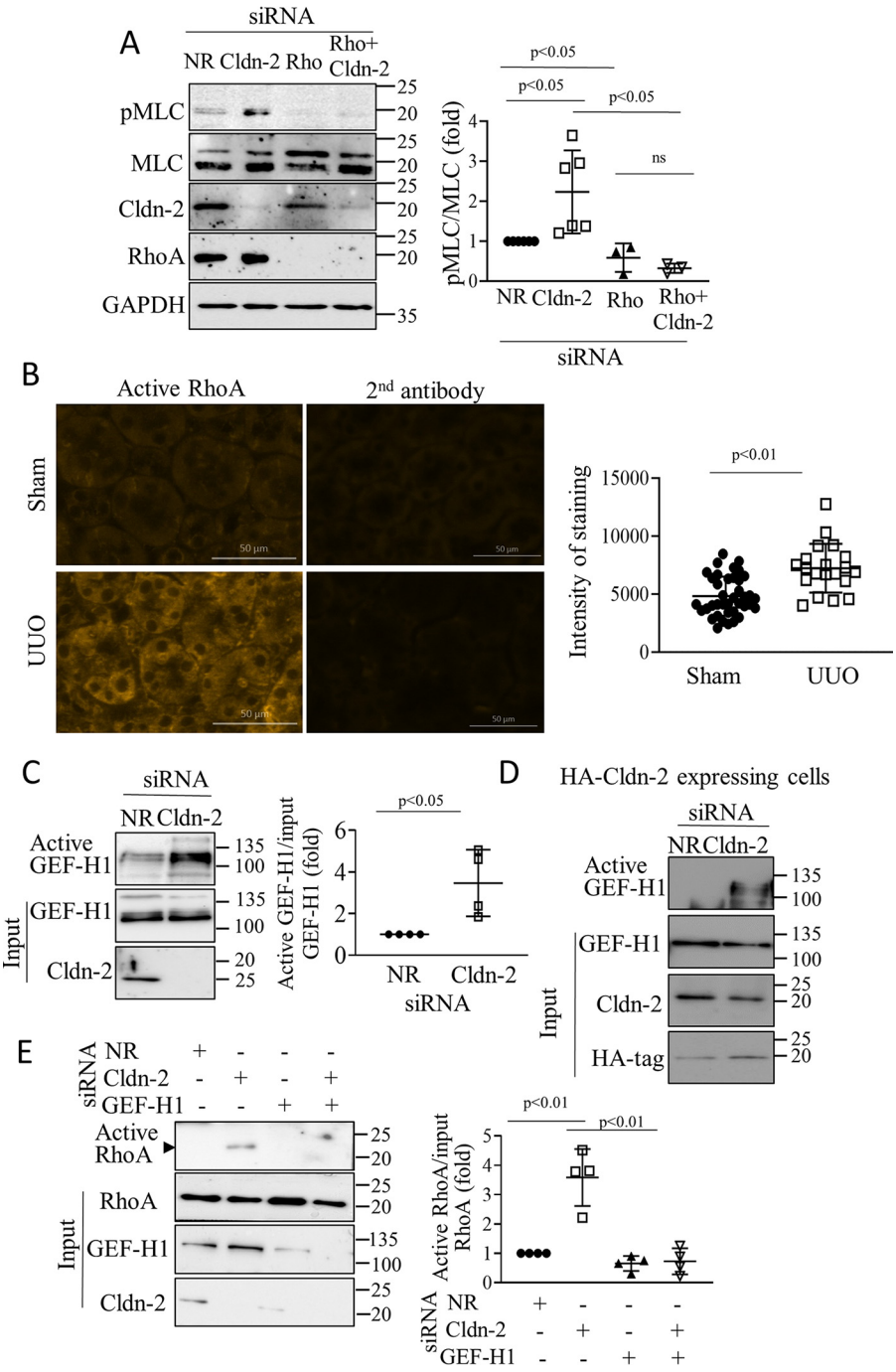

Figure 4. *A*, Cldn-2 silencing activates pMLC through RhoA. LLC-PK$_1$ cells were transfected with NR or claudin-2–specific siRNA with or without RhoA-specific siRNA, and 48 h later the cells were lysed, and phospho-MLC was detected and quantified by Western blotting as in Fig. 2 (means ± S.D., $n = 3–6$). *B*, active RhoA is elevated in UUO. The mice were sham-operated or underwent UUO (7 days), as in Fig. 1. Active RhoA was detected in renal tissue sections by immunofluorescent staining with a RhoA-GTP–specific antibody as in Fig. 3. The *right images* show labeling with the secondary antibody alone. *Bar*, 50 μm. Intensity of the labeling was quantified using the Zen software in regions of 100-μm diameter (>30 regions/animals in three animals in each group). Average labeling in samples exposed to the secondary antibody only was subtracted from each intensity value (means ± S.D.) *C–E*, Claudin-2 silencing activates RhoA through GEF-H1. *C* and *D*, WT or HA–CLDN-2 expressing LLC-PK$_1$ cells were transfected with NR or Cldn-2–specific siRNA, and 48 h later they were lysed, and active GEFs were precipitated using GST–RHOAG17A. Captured (active) and input (total) GEF-H1 was detected by Western blotting. The input cell lysates were redeveloped with Cldn-2 antibody to verify silencing. Active GEF-H1 values were normalized to the input GEF-H1 (means ± S.D., $n = 4$). *E*, WT LLC-PK$_1$ cells were transfected with NR or Cldn-2–specific siRNAs with or without GEF-H1 siRNA, and active RhoA was precipitated and quantified as in Fig. 3 (means ± S.D., $n = 4$).

unique feature of LLC-PK$_1$ cells, we repeated these experiments in the distal tubule cell line MDCK. As shown on Fig. 3*B*, CLDN-2 silencing in MDCK cells also resulted in elevated RHOA activity. Importantly, CLDN-2 siRNA did not induce RHOA activation in LLC-PK$_1$ cells expressing an siRNA-resistant HA-tagged mouse CLDN-2 (Fig. 3*C*), verifying that the effect was indeed due to loss of CLDN-2 protein. Moreover, RHOA activation was not a general phenomenon caused by loss of any claudin, because neither Cldn-1 nor Cldn-7 silencing altered RHOA activity (Fig. 3*D*).

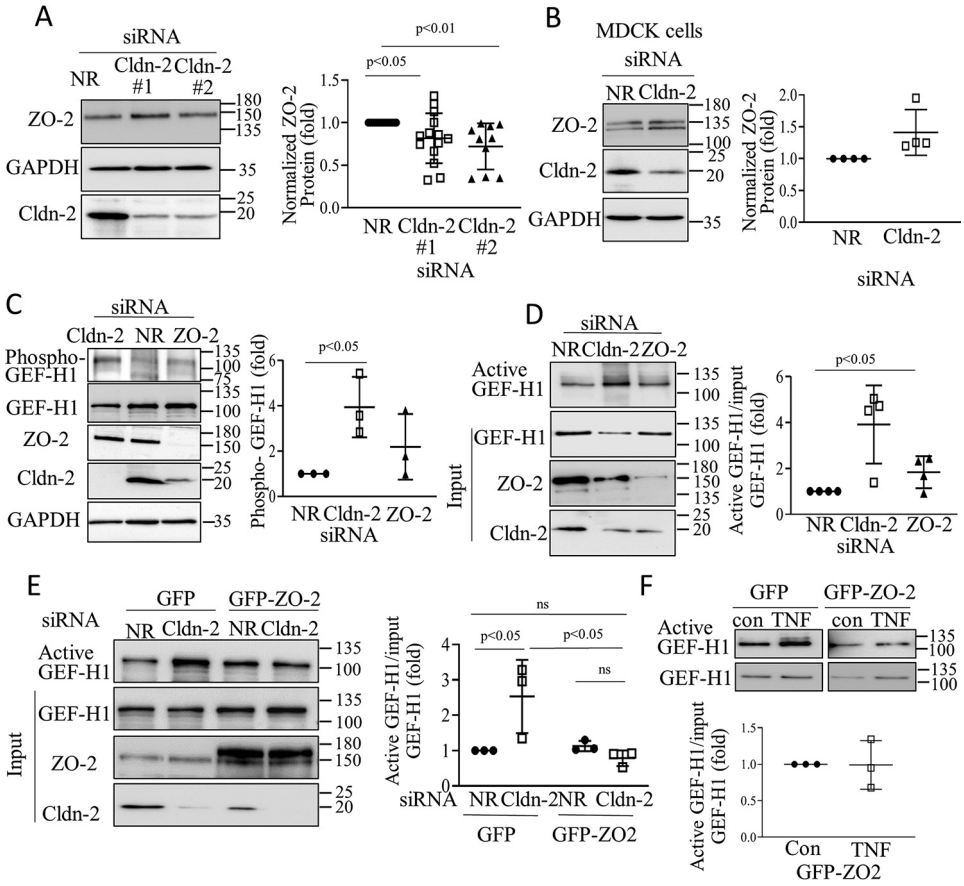

Figure 5. *A* and *B*, LLC-PK$_1$ (*A*) or MDCK (*B*) cells were transfected with NR or Cldn-2 siRNA, and 48 h later the indicated proteins were detected by Western blotting. The corresponding graphs show ZO-2 normalized with GAPDH (fold from NR siRNA transfected control) (means ± S.D.; in *A*, $n = 14$ and 12 for the two siRNAs, respectively; in *B*, $n = 4$). *C* and *D*, LLC-PK$_1$ cells were transfected with NR or Cldn-2 or ZO-2 siRNA as indicated. In *C*, phospho-GEF-H1 was detected and quantified using an antibody against pSer-885 GEF-H1. The graph shows the phospho–GEF-H1 signal normalized to total GEF-H1 and expressed as fold over control. In *D*, 48 h after transfection, active GEF-H1 was detected and quantified as earlier (means ± S.D., $n = 3$). The indicated proteins were also detected in total cell lysates. *E* and *F*, LLC-PK$_1$ cells expressing GFP–ZO-2 or the eGFP control vector were transfected with NR or Cldn-2 siRNA (*E*) or treated with 10 ng/ml TNFα for 10 min (*F*). Active GEF-H1 was detected and quantified as earlier (means ± S.D., $n = 3$). The indicated proteins were also detected in total cell lysates.

Next, we explored how loss of CLDN-2 affected RHOA activity in kidneys of a CLDN-2 KO mouse. We used an active RHOA-specific antibody to stain kidney sections obtained from WT or CLDN-2 KO mice, as in our earlier study (35). Immunofluorescent staining with this antibody and the corresponding quantification (Fig. 3*E*) revealed increased labeling localized mostly in the tubules in the KO mice. Thus, loss of CLDN-2 results in elevated RHOA activity in tubular cells both *in vitro* and *in vivo*.

We next asked whether CLDN-2 depletion elevated pMLC through RHOA. We used a RHOA-specific siRNA, as in previous studies (19) that efficiently down-regulated RHOA (Fig. 4*A*). RHOA silencing reduced basal pMLC and prevented the increase caused by CLDN-2 siRNA.

We have previously demonstrated that RHOA was activated in the kidney tubules in the UUO fibrosis model as early as 1 day after ligation of the ureter (35). To assess whether this activation was sustained, we used the active RHOA-specific antibody in 7-day UUO samples (35). Immunofluorescent staining revealed increased labeling localized mostly in the tubules (Fig. 4*B*). Thus, RHOA activation is sustained in a pro-fibrotic animal model concomitant with CLDN-2 down-regulation.

Claudin-2 silencing activates RHOA through the exchange factor GEF-H1

Next, we sought to determine how CLDN-2 silencing activated RHOA. GEF-H1 is an epithelial guanine nucleotide exchange factor that binds to microtubules (39) and the intercellular junctions (40, 41). In tubular cells GEF-H1 mediates cytokine-induced RHOA activation (9, 38). To assess whether CLDN-2 down-regulation affected GEF-H1, we performed an affinity precipitation assay using GST–RHOAG17A (9) that binds activated GEFs with high affinity. Active GEFs were precipitated from tubular cells transfected with NR or CLDN-2–specific siRNA and assessed by Western blotting. Although some active GEF-H1 was detectable in control, the level of active GEF-H1 significantly increased upon CLDN-2 silencing (Fig. 4*C*). In cells transfected with siRNA-resistant HA–CLDN-2, basal GEF-H1 activity was lower, and CLDN-2 silencing caused reduced GEF-H1 activation (Fig. 4*D*). Importantly, GEF-H1 was required for RHOA activation induced by CLDN-2 depletion, because silencing GEF-H1 along with CLDN-2 prevented this effect (Fig. 4*E*).

ZO-2 silencing was recently shown to activate RHOA through GEF-H1 (8). Therefore, we next asked whether

CLDN-2 depletion altered ZO-2 expression. As shown on Fig. 5*A*, CLDN-2 depletion with either of the siRNAs caused a modest (~25%) but significant drop in ZO-2 levels in LLC-PK^1 cells. In contrast, no change was observed in ZO-2 expression in MDCK cells (Fig. 5*B*), despite efficient CLDN-2 silencing. Thus, there was no clear correlation between the ability of the CLDN-2 siRNA to activate RHOA and to induce a drop in ZO-2 levels. We next assessed the effect of CLDN-2 silencing on GEF-H1 phosphorylation at Ser-885, which was shown to increase GEF-H1 activity (38, 42). As shown of Fig. 5*C*, CLDN-2 silencing caused a substantial and significant increase in GEF-H1 Ser-885 phosphorylation, whereas ZO-2 silencing caused only a marginal and nonsignificant effect. Moreover, CLDN-2 silencing caused much stronger GEF-H1 activation than ZO-2 silencing, a finding concordant with their differential effect on GEF-H1 phosphorylation (Fig. 5*D*). Finally, we generated an LLC-PK$_1$ cell line expressing GFP–ZO-2. Silencing CLDN-2 in the control cells caused a well-detectable GEF-H1 activation. In contrast, in the GFP–ZO-2– expressing cells, CLDN-2 silencing no longer caused GEF-H1 activation (Fig. 5*E*). We tested the effects of acute TNFα treatment, a strong activator of GEF-H1. Of note, at this time point (10 min), TNFα does not reduce CLDN-2 expression (19). Surprisingly, in cells overexpressing GFP–ZO-2 TNFα failed to elicit GEF-H1 activation (Fig. 5*F*). Thus, overexpression of ZO-2 likely exerts a general inhibitory effect on GEF-H1 activation. Taken together, our data imply that although ZO-2 might contribute to a limited extent to GEF-H1 activation induced by CLDN-2 depletion, additional mechanisms must also contribute (see discussion on this point). Taken together, CLDN-2 specifically suppresses GEF-H1 and RHOA activity, and its down-regulation leads to GEF-H1-dependent RHOA activation and consequent increase in cell contractility.

CLDN-2 silencing reduces proliferation in tubular cells

CLDN-2 promotes proliferation in cancer cells (23). We next wished to test whether a similar effect exists in tubular cells. First, electric cell-substrate impedance sensing (ECIS) was used to follow the development of the epithelial layer with or without CLDN-2. Capacitance measurements at high frequency with ECIS reflect electrode coverage and thus can be used to measure cell proliferation (43, 44). For these measurements equal numbers of LLC-PK$_1$ cells transfected with NR of CLDN-2–specific siRNA were plated on ECIS electrodes, and capacitance (*C*) was measured continuously, as in Ref. 38. The cell number was chosen so that the initial layer was subconfluent. Thus, capacitance decrease after the initial adhesion reflects cell growth and the development of a confluent layer (38). When the layer becomes confluent, *C* reaches a minimum. As shown on Fig. 6*A*, CLDN-2 silencing resulted in a slower drop in *C*. In fact, over several measurements, the time for reaching 50% capacitance drop was significantly higher when CLDN-2 was silenced (Fig. 6*A*, *right panel*), suggesting a slower proliferation rate. Nevertheless, the drop in *C* suggested that the cells did proliferate and reached confluence even when CLDN-2 was silenced. To test the impact of CLDN-2 silencing on proliferation with an alternative method, we stained cells transfected with control or CLDN-2–specific siRNA for Ki67, an indicator of proliferation. We found that CLDN-2 silencing reduced the number of Ki67-positive cells (Fig. 6*B*). Contact inhibition reduces proliferation of LLC-PK$_1$ cells as they reach confluence; however, a recently confluent LLC-PK$_1$ cell layer can still respond to proliferative stimuli (45). In fact, we showed that TNFα augmented proliferation through transactivation of the EGF receptor (45). As shown on Fig. 6*C*, expression of the proliferation marker proliferating cell nuclear antigen (PCNA) was low in a serum-deprived confluent layer but was augmented by 24-h treatment with serum or TNFα, indicating that a portion of cells re-enter the cycle under these conditions. This effect, however, was markedly reduced in cells transfected with CLDN-2 siRNA. To obtain a more quantitative assessment of cell cycle progress, we determined BrdU incorporation, a measure of DNA synthesis during the S phase. In line with a lower proliferation rate, CLDN-2 silencing reduced basal BrdU incorporation (Fig. 6*D*). Further, TNFα elevated BrdU incorporation in cells transfected with the nonrelated siRNA, but this effect was significantly blunted in cells transfected with CLDN-2 siRNA (Fig. 6*D*). To further verify that CLDN-2 modifies proliferation, we used an LLC-PK$_1$ cell line with stable overexpression of HA–CLDN-2. These cells showed slightly but significantly elevated basal and TNFα-induced BrdU incorporation (Fig. 6*E*). Importantly, neither Cldn-1 nor Cldn-7 silencing altered basal and TNFα-stimulated BrdU incorporation (Fig. 6*F*). Taken together, CLDN-2 loss reduced, whereas CLDN-2 increase augmented cell proliferation.

CLDN-2 silencing reduces proliferation through RHOA-dependent up-regulation of P27KIP1

Cell cycle control involves the coordinated regulation of cyclin-dependent kinases by cyclins and cyclin-dependent kinase inhibitors (CDKI) (46). As shown in Fig. 7*A*, CLDN-2 silencing in tubular cells significantly up-regulated the Cip/Kip family CDKI, P27KIP1 (cyclin-dependent kinase inhibitor 1B). This protein blocks transition from the G$_1$ to S phases, and thus it reduces proliferation. The increase in P27KIP1 was prevented by simultaneous silencing of RHOA (Fig. 7*A*). We also assessed the role of GEF-H1. The cells were transfected with a GEF-H1–specific siRNA (38) that caused ~50% down-regulation of the protein (Fig. 7*B*). As reported by us earlier (33) GEF-H1 silencing reduced CLDN-2 expression. Importantly, down-regulating GEF-H1 along with CLDN-2 prevented the increase in P27KIP1 caused by CLDN-2 silencing (Fig. 7*B*). These data suggest that CLDN-2 alters proliferation through GEF-H1/RHOA. Silencing of CLDN-2 also up-regulated P27KIP1 in MDCK cells (Fig. 7*C*), indicating that the effect was not unique to LLC-PK$_1$ cells. In many scenarios RHOA promotes rather than inhibits proliferation, although anti-proliferative effects were also demonstrated (47). To verify that RHOA activation indeed can reduce proliferation in LLC-PK$_1$ cells, we used Rho activator II, a cell-permeable toxin that activates Rho GTPases by deamidating glutamine 63. Treatment of LLC-PK$_1$ cells with this toxin significantly reduced BrdU incorporation (Fig. 7*D*). To assess the role of P27KIP1 as a

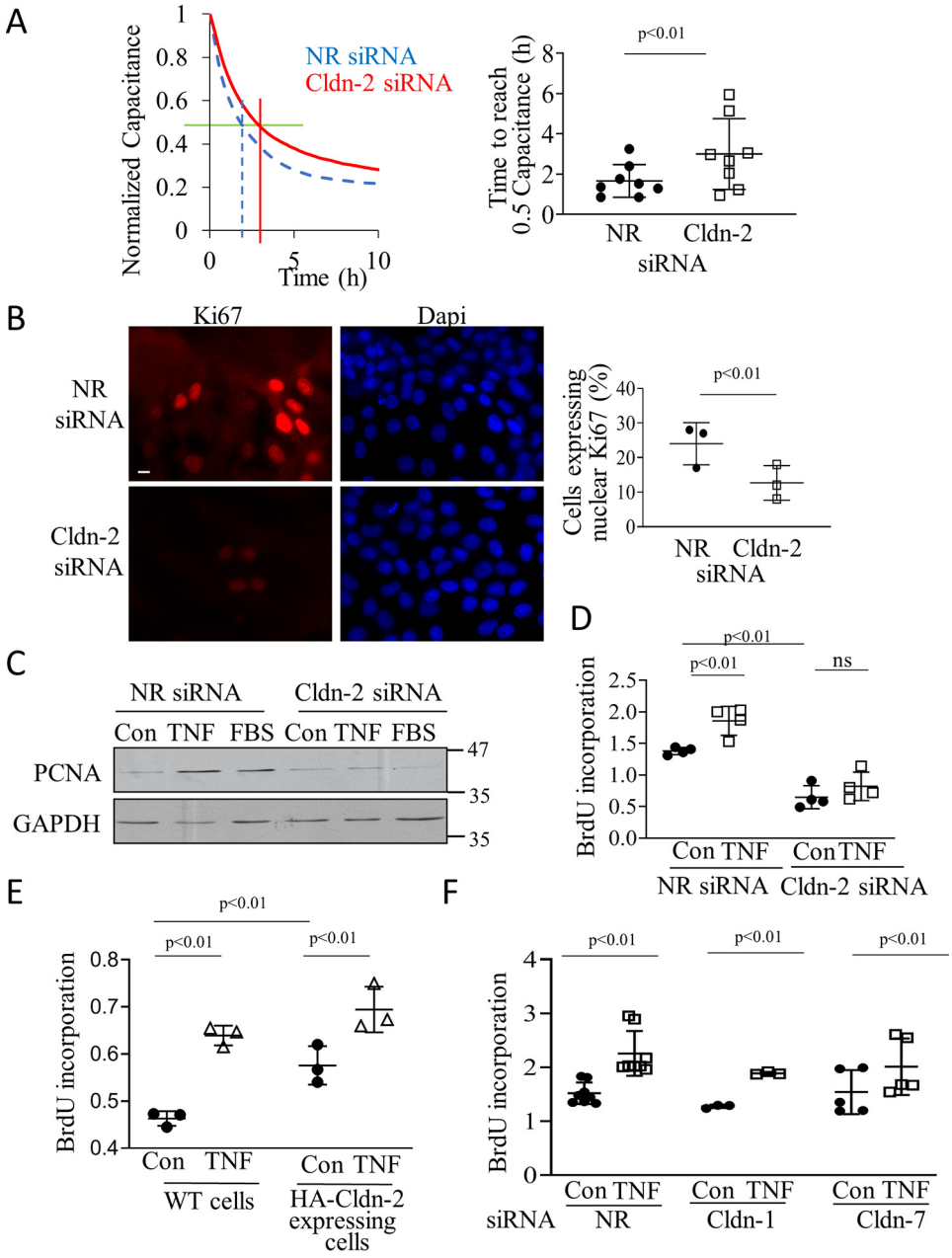

Figure 6. Claudin-2 down-regulation reduces basal and TNFα-induced proliferation. *A*, LLC-PK$_1$ cells were transfected with NR (*blue dashed line*) or Cldn-2 (*red solid line*) siRNA. 24 h later cells were trypsinized and seeded on 8W10E array ECIS electrodes. Capacitance (*C*) was continuously monitored at 32 kHz. The *left graph* shows a typical measurement of $n = 3$ (in duplicate). Average of two parallel measurements/conditions is shown. The values were normalized to the first measurement point. The *green horizontal line* indicates 0.5 capacitance, and the *red* and *blue* (*dashed*) *vertical lines* indicate corresponding time. The *right graph* shows the time required to reach the 0.5 capacitance value (means ± S.D., $n = 4$ measurements in duplicate). *B*, LLC-PK$_1$ cells grown on coverslips were transfected with NR or Cldn-2–specific siRNA, and 48 h later, after reaching confluence, they were fixed and stained using a Ki67-specific antibody and DAPI. Pictures were obtained using Olympus IX81 epifluorescent microscope. Ki67-positive cells were counted using the Metamorph software and expressed as the percentage of total (DAPI-positive) nuclei. The average of ten fields in three coverslips/treatment are shown (means ± S.D., $n = 3$). The *bar* represents 10 μM and applies to all the images. *C*, LLC-PK$_1$ cells transfected with NR or Cldn-2–specific siRNA were grown for 24 h and then serum-depleted overnight. Next, 20 ng/ml TNFα or 10% FBS was added for 16 h. PCNA was detected by Western blotting with GAPDH as loading control. *D–F*, WT or HA–CLDN-2 expressing (*E*) LLC-PK$_1$ cells were transfected with NR, Cldn-1, -2, or -7–specific siRNAs, as indicated. The cells were grown in 96-well plates to ≈90% confluence, serum-depleted overnight, and treated with 20 ng/ml TNFα for 16 h in the presence of BrdU. BrdU incorporation was quantified using a colorimetric ELISA kit (means ± S.D.; in *D*, $n = 4$; in *E*, $n = 3$; in *F*, $n = 5–6$, performed in triplicate). *ns*, nonsignificant *versus* NR siRNA control.

mediator of the effects of CLDN-2 silencing, we simultaneously silenced CLDN-2 and P27KIP1. The P27KIP1-specific siRNA efficiently reduced the protein and prevented its increase upon CLDN-2 silencing (Fig. 7*E*, *right panel*). When cells were transfected with the P27KIP1 siRNA close to confluence, it did not interfere with the development of a confluent layer and had no effect on basal BrdU incorporation (Fig. 7*E*). Importantly, when P27KIP1 was silenced, loss of CLDN-2 no longer reduced BrdU incorporation. Two different P27KIP1siRNAs had similar effects.

Finally, we also assessed expression of P27KIP1 in the UUO model. As shown on Fig. 7*F* immunohistochemical staining

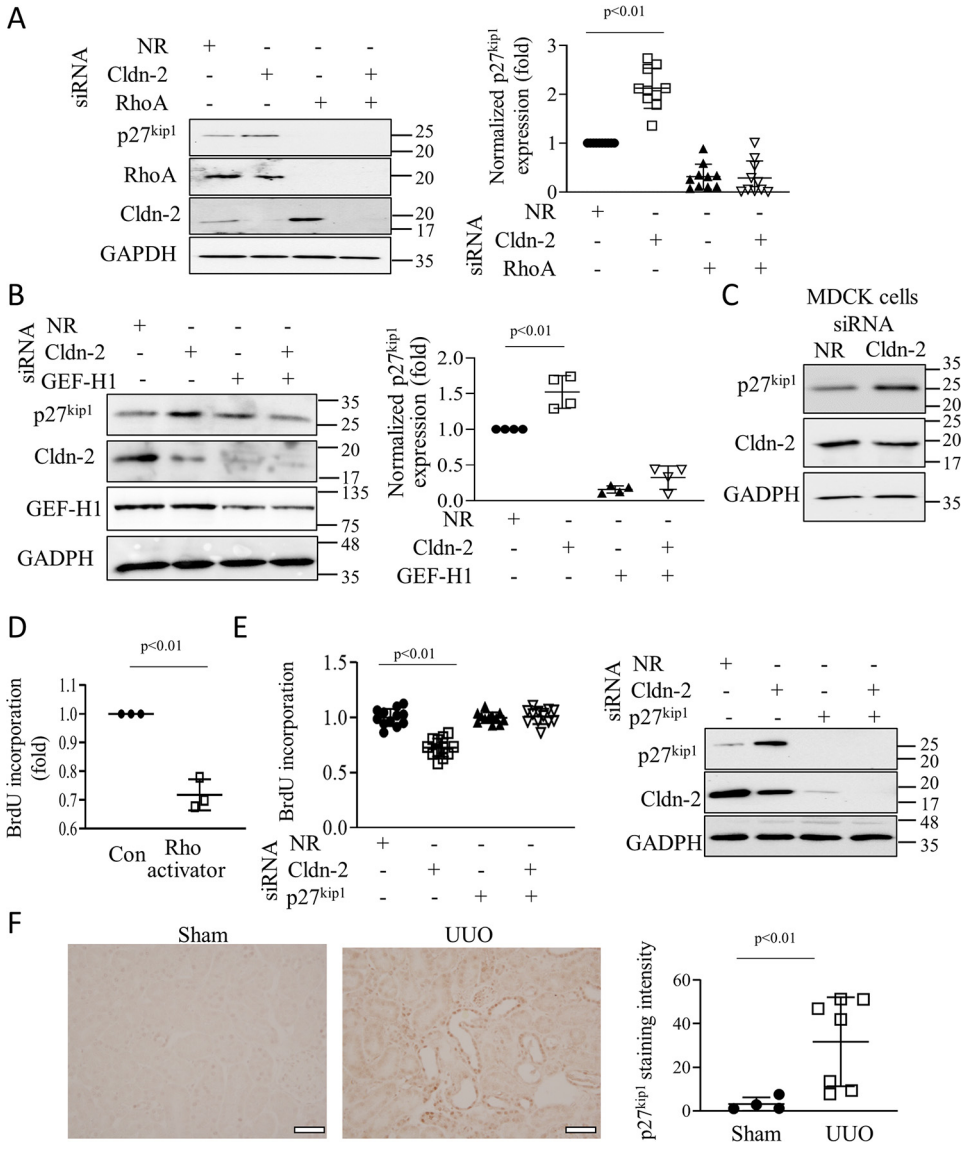

Figure 7. Claudin-2 silencing slows proliferation through GEF-H1/RhoA-dependent up-regulation of p27^{kip1}. *A–C*, LLC-PK$_1$ (*A* and *B*) or MDCK (*C*) cells were transfected with NR, Cldn-2, RhoA, or GEF-H1–specific siRNA, and the indicated proteins were detected and quantified by Western blotting. *D*, RhoA activation reduces proliferation. Confluent LLC-PK$_1$ cells were treated with 0.25 mg/ml Rho activator II for 16 h, and BrdU incorporation was measured as in Fig. 6. Graphs show means ± S.D. In *A*, $n = 10$; in *B*, $n = 4$; and in *D*, $n = 3$. *E*, LLC-PK$_1$ cells were transfected with NR or Cldn-2–specific siRNA with or without p27^{kip1} siRNA, as indicated, and BrdU incorporation was measured. In parallel experiments, silencing was verified by Western blotting (means ± S.D., $n = 12$). *F*, mice were sham-operated or underwent UUO (7 days), as described in Fig. 1. Renal tissue sections were processed for immunohistochemistry using a primary antibody against p27^{kip1}. Quantification was done as described under "Experimental procedures" ($n = 5$ and 7 random areas in 2 animals). *Bar*, 50 μm.

revealed a substantial and significant increase in the tubular levels of P27KIP1. Taken together, these data show that CLDN-2 silencing reduces proliferation through a GEF-H1 and RHOA-dependent increase in the CDKI P27KIP1.

CLDN-2 silencing activates the MRTF/SRF pathway and promotes pro-fibrotic changes

RHOA signaling plays a central role in the development of a profibrotic epithelial phenotype (PEP) (35). This process is brought about by a major transcriptional reprogramming, which results in epithelial fibrogenic cytokine production. It also manifests in a departure from the classic epithelial phenotype, resulting in partial and sometimes complete epithelial–mesenchymal transition (EMT) or epithelial myofibroblast transition (48). MRTF is a co-factor of SRF and the MRTF/SRF complex is a crucial RHOA-regulated mediator of PEP and EMT (49). To assess whether MRTF/SRF are affected by CLDN-2, we used the CARG-box containing reporter 3DA promoter (50). Transfection with CLDN-2 siRNA elevated the activity of this promoter construct compared with the control siRNA (Fig. 8*A*). Importantly, this effect was absent in cells expressing the siRNA-resistant HA–CLDN-2. In addition, the promoter was less active when CLDN-2 was overexpressed (*i.e.* in the HA–CLDN-2 cells), further supporting a role for CLDN-2 as a negative regulator of MRTF/SRF. The effect of CLDN-2 siRNA on the reporter was mediated by RHOA, because promoter activation was prevented by the RHOA inhibitor Rhosin (Fig. 8*B*). MRTF can be phosphorylated on multiple sites (51), a subset of which results in activation. To test whether CLDN-2 silencing also affected phosphorylation,

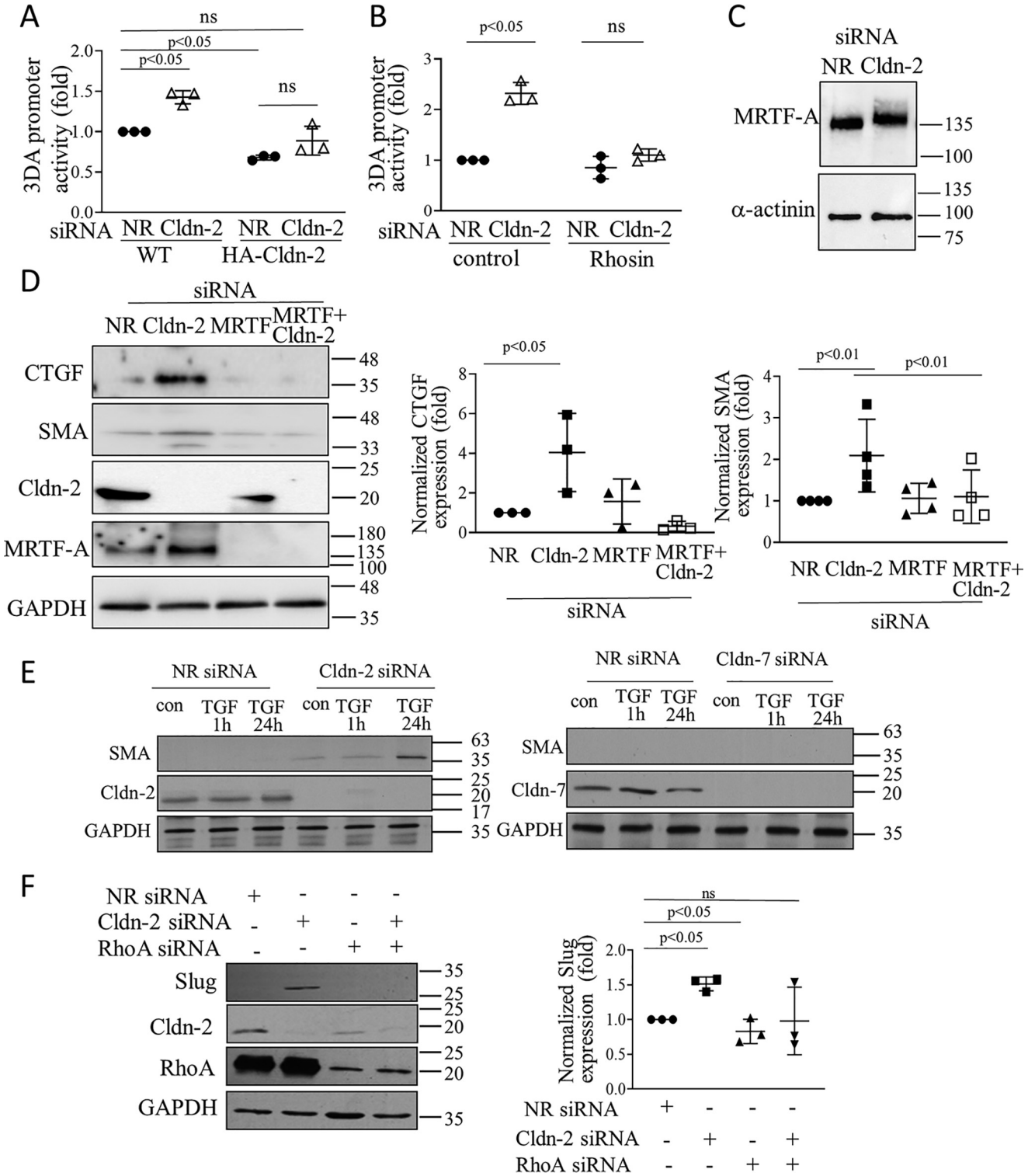

Figure 8. Cldn-2 silencing activates MRTF and enhances pro-fibrotic changes in tubular cells. *A* and *B*, WT or HA–CLDN-2 expressing LLC-PK$_1$ cells were transfected with a firefly luciferase-coupled MRTF/SRF sensitive promoter (3DA), along with the internal control pRL-TK (*Renilla* luciferase). In *A*, the cells were also transfected with NR or Cldn-2–specific siRNA. *B*, cells were treated with the Rho inhibitor Rhosin (24 h, 30 μM). 24 h post-transfection luciferase activity was determined using the Dual-Luciferase assay kit. Firefly luciferase activity was normalized using the *Renilla* luciferase activity and expressed as fold change from control (means ± S.D., $n = 3$) *C*, whole cell extracts were separated on 6% SDS gels to detect the relative shift in MRTF-A molecular mass with α-actinin as loading control. *D*, LLC-PK$_1$ cells were transfected with Cldn-2 or MRTF-A–specific siRNAs, or both, as indicated. CTGF and SMA were detected and quantified (means ± S.D., $n = 3$). The blots were developed for Cldn-2 and MRTF-A to verify silencing. *E* and *F*, LLC-PK$_1$ cells were transfected with siRNAs and treated with 10 ng/ml TGFβ1 for 1 h (in *E*) or 24 h (*E* and *F*), and the indicated proteins were detected. Note that the two blots in *E* were run parallel, and thus the left blots serve as control for detectability of SMA expression. In *F*, graph shows means ± S.D., $n = 3$.

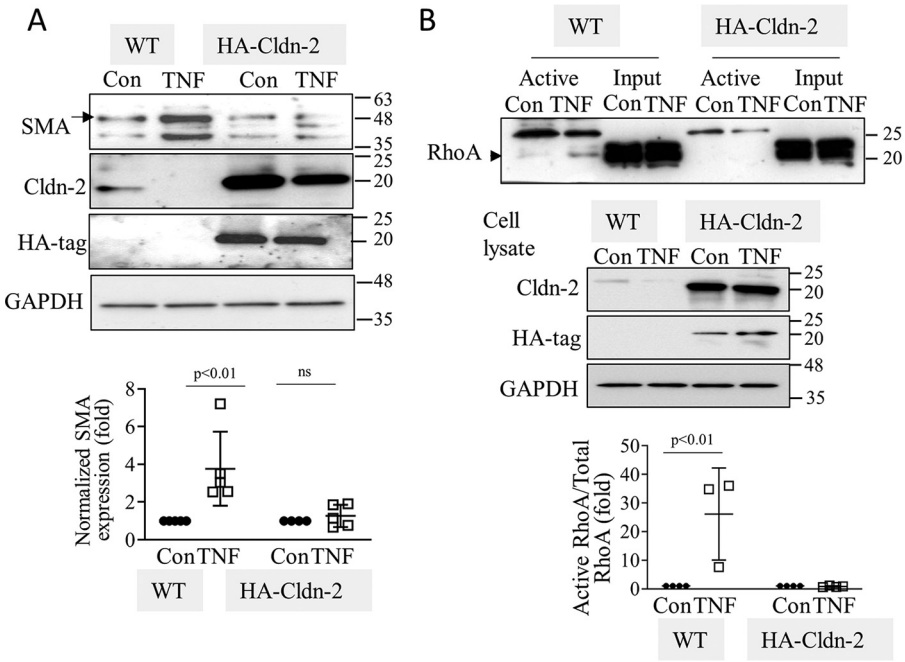

Figure 9. Claudin-2 down-regulation by TNFα is a requisite for increased SMA expression and sustained RhoA activation. WT or HA–CLDN-2 transfected LLC-PK$_1$ cells were treated with 20 ng/ml TNFα for 24 h. In *A*, the indicated proteins were detected by Western blotting. In *B*, active RhoA was precipitated and detected as in Fig. 3. In *A*, the *arrow* points to SMA (42 kDa), and in *B*, the *arrowhead* indicates RhoA. The blots were quantified as earlier (means ± S.D., $n = 5$ (*A*) and 3–5 (*B*)).

we detected changes in MRTF mobility on SDS gels, reflecting the presence of phosphorylated species, as in Ref. 50. CLDN-2 silencing caused an upward shift in the apparent molecular weight of MRTF, indicative of post-translational modification, most likely phosphorylation (Fig. 8*C*).

Next, we asked whether activation of MRTF upon CLDN-2 depletion indeed might lead to PEP. Therefore, we explored the expression of connective tissue growth factor (CTGF), a main pro-fibrotic cytokine regulated by MRTF (35, 52). Indeed, silencing claudin-2 by itself elevated CTGF expression (Fig. 8*D*). As expected, this effect was MRTF-dependent.

Confluent LLC-PK$_1$ cells express only low levels of the myofibroblast marker smooth muscle actin (SMA). Moreover, TGFβ1, a strong inducer of EMT, is insufficient to promote complete fibrotic reprogramming in an intact (confluent) epithelial layer, unless a second hit (*e.g.* injury) to the cell contacts is also present (53, 54). As shown on Fig. 8*D*, CLDN-2 silencing by itself caused a small but significant increase in SMA expression. Moreover, this effect was MRTF-dependent, because co-transfection of an MRTF-A siRNA prevented it. Further, in line with previous studies, TGFβ1 did not induce SMA expression in control cells (Fig. 8*E*). In contrast, prolonged (24 h) treatment with TGFβ strongly elevated SMA when CLDN-2 was silenced (Fig. 7*E*). No similar augmentation was present on Cldn-7 silencing (Fig. 7*E*). Finally, we also assessed whether other PEP/EMT-promoting transcription factors were affected by CLDN-2 silencing. As shown in Fig. 8*F*, CLDN-2 silencing up-regulated Slug (Snail2) in a RHOA-dependent manner. Taken together, these findings support an EMT suppressor role for CLDN-2 and suggest that its loss promotes epithelial reprogramming.

TNFα-induced CLDN-2 down-regulation is a requisite for the RHOA-activating effect of TNFα

In the final series of experiments, we wished to explore whether TNFα-induced down-regulation of CLDN-2 contributes to the prolonged effects of this cytokine on SMA production and RHOA activation. To this end, we compared SMA expression in TNFα-treated WT or HA–CLDN-2 expressing cells. In line with our previous findings, 24 h of TNFα treatment potently reduced CLDN-2 levels in WT LLC-PK$_1$ cells (Fig. 9*A*, *left two lanes*). TNFα had significantly less effect on HA–CLDN-2, driven by an artificial promoter (Fig. 9*A*, *right two lanes*). Long-term TNFα stimulation significantly augmented SMA expression in WT LLC-PK$_1$ cells, but not in the HA–CLDN-2 expressing cells, where CLDN-2 was still present. Further, affinity precipitation of active RHOA showed that 24 h of TNFα stimulation induced RHOA activation only in WT LLC-PK$_1$ cells, but not in cells overexpressing HA–CLDN-2, where CLDN-2 was still detectable (Fig. 9*B*). Taken together, our data support that prolonged TNFα down-regulates CLDN-2, which is required for RHOA activation.

Discussion

The central finding of this study is that CLDN-2 is a negative regulator of RHOA. Accordingly, CLDN-2 loss induced by cytokines can lead to GEF-H1–dependent RHOA activation, which mediates up-regulation of the CDKI P27KIP1 to reduce proliferation. Additionally, CLDN-2 loss can enhance RHOA-mediated activation of MRTF to promote profibrotic reprogramming.

Inflammation affects CLDN-2 in a tissue-dependent manner. Although CLDN-2 expression is up-regulated in inflam-

matory bowel disease (55), TNFα down-regulates CLDN-2 in tubular cells (19). We showed that in a mouse kidney injury model, CLDN-2 levels initially rose, followed by a drop. This is in line with the effect of TNFα in tubular cells (19). In the 3-day UUO condition, both CLDN-2 mRNA and protein increased, suggesting augmented transcription/translation. In contrast, in the 7-day UUO only CLDN-2 protein but not mRNA dropped significantly below basal levels. Our data argue against a general loss of tubules as the cause of the late drop in CLDN-2 protein. This conclusion is supported by the fact that we found no change in expression of CLDN-2 or SGLT-2 mRNA, which are proximal tubular proteins. Further, several tubular markers were also unchanged in UUO, as measured using LCM. Instead, CLDN-2 protein down-regulation is likely the result of augmented degradation. The mechanisms of CLDN-2 expression changes during kidney injury, however, remain undefined and warrant further studies.

We suggest that in resting epithelial cells CLDN-2 is a suppressor of the RHOA pathway. This notion is supported by experiments using CLDN-2 silencing and overexpression in tubular cells and by the demonstration of elevated active RHOA levels in the kidneys of CLDN-2 KO mice.

In our previous study we found that CLDN-2 silencing elevated TER (19). In fact, increased TER as a result of claudin-2 depletion is well-established in the literature (18, 31, 56). In the current study we report increased RHOA activity and pMLC levels caused by CLDN-2 depletion. It is well-established that pMLC promotes TJ protein endocytosis and junction disruption induced by various stimuli. Thus, simultaneous increases in TER and pMLC may appear to be contradictory. However, there is compelling evidence in the literature that these parameters can increase in parallel, consistent with our findings. For example, stable ZO-2 KD in an MDCK cell line resulted in RHOA activation, as well as CLDN-2 decrease and TER increase (8). Further, in lung epithelial cells thrombin produced prominent circumferential localization of actin fibers and elevated both MLC phosphorylation and TER, resulting in barrier protection (57). In endothelial cells sphingosine-1-phosphate, a strong RHOA activator was shown by multiple studies to induce endothelial barrier enhancement, mediated by RHOA, along with increased peripheral pMLC (58–60). How can these discordant findings be reconciled? Fine spatiotemporal control of RHOA and pMLC may be the key to the overall outcome. Interestingly, in endothelial cells, RHOA activation at the cell periphery correlates with barrier integrity, whereas its activation in the perinuclear area contributes to barrier disruption (61). Together, these findings imply that the role of RHOA and pMLC in TJ regulation is complex. Although pMLC is required for endocytosis of TJ proteins and contributes to the disruption of TJs, pMLC is also vital for the formation of adherens and tight junctions (62, 63). The role of increased pMLC upon CLDN-2 depletion remains to be further studied.

Rho family proteins are under tight spatiotemporal control by numerous regulators, several of which can bind to TJs (4). We suggest that the negative effect of CLDN-2 on RHOA signaling in resting cells is due to suppression of GEF-H1. This conclusion is based on the following evidence. A GEF affinity precipitation assay (9, 64) revealed that CLDN-2 silencing caused an increase in GEF-H1 activity. We also found augmented phosphorylation on Ser-885. Importantly, GEF-H1 silencing blunted RHOA activation induced by CLDN-2 depletion. GEF-H1 was first described as a microtubule-bound protein involved in microtubule–actin cross-talk (39). Subsequently, it was shown to bind the TJ-associated adapters cingulin and paracingulin that inhibit its activity (6, 7). GEF-H1 affects a wide range of processes including cytokinesis (65), mechanotransduction (66), migration (38, 67), junction formation (41), and vesicle trafficking (68). Thus, GEF-H1 activation by CLDN-2 loss could lead to significant changes in a range of epithelial functions. The mechanism through which CLDN-2 controls GEF-H1 remains to be elucidated. Sequestration of GEF-H1 at the TJs by cingulin or paracingulin could play a role (6, 7). In a recent paper Raya-Sandino *et al.* (8) showed that ZO-2 down-regulation induced cingulin and GEF-H1 phosphorylation and activated GEF-H1/RHOA. We explored the effects of CLDN-2 silencing on ZO-2 levels and found no strong correlation between the magnitude of ZO-2 reduction and GEF-H1 activation. Specifically, the two CLDN-2 siRNAs caused relatively modest (and somewhat variable) ZO-2 reduction in LLC-PK$_1$ cells (up to 25%) but provoked stronger GEF-H1 activation than direct and robust ZO-2 down-regulation. In contrast, CLDN-2 silencing did not reduce ZO-2 in MDCK cells, although it induced strong RHOA activation. Further, whereas CLDN-2 silencing significantly elevated GEF-H1 phosphorylation, ZO-2 silencing caused only a weak, nonsignificant rise, despite a substantial drop in ZO-2 expression. Taken together, these data strongly argue that ZO-2 is not the major mediator of GEF-H1 activation upon CLDN-2 silencing. Interestingly, however, in a cell line expressing GFP–ZO-2, CLDN-2 depletion no longer activated GEF-H1. In these cells TNFα, a strong activator of GEF-H1 also failed to promote GEF-H1 activation, under conditions where it did not affect CLDN-2 levels (9, 19). This suggests that ZO-2 overexpression exerts a general suppressive effect on GEF-H1 activation. In aggregate, our findings imply that although ZO-2 reduction cannot be excluded as a potential contributor to the overall effect, the participation of additional mechanisms linking CLDN-2 depletion to GEF-H1 activation is very likely. The mechanisms through which CLDN-2 affects ZO-2 are currently unknown. Interestingly, ZO-2 and CLDN-2 mutually regulate each other's expression, because ZO-2 silencing induces a reduction in CLDN-2 (8, 69). Thus, ZO-2 and CLDN-2 could regulate each other's stability, and both could be required for suppressing GEF-H1/RHOA.

Interestingly, CLDN-2 silencing strongly promoted GEF-H1 phosphorylation on Ser-885, which may be a key step in its activation (38, 42). GEF-H1 can be phosphorylated by a variety of kinases, including ERK, PAK, Aurora A, and GSK, and this controls its activation (reviewed in Ref. 39). We found that in tubular cells TNFα-induced ERK-dependent phosphorylation on Thr-678 was necessary for RHOA activation, whereas Ser-885 affected both RHOA and Rac exchange activity (38). Of note, we did not find evidence that CLDN-2 depletion altered ERK activity (not shown). Microtubule binding also controls GEF-H1. Thus, possible changes in TJ-associated microtubules induced by CLDN-2 depletion also warrant assessment. Cingulin binds the TJ-associated apical microtubule network (70).

Whether CLDN-2 interacts with this network is currently not known.

Small GTPases are controlled by a multitude of inputs. Therefore, the relative contribution of CLDN-2 in RHOA activation during inflammatory diseases is difficult to establish. We recently found strong RHOA activation in the UUO model as early as 1 day after the injury (35), This is likely due to the presence of numerous early stimuli, including acute mechanostress. At later time points, however, prolonged loss of CLDN-2 might be one of the factors that promotes sustained RHOA activation. Our current findings showing elevated RHOA activity in the kidneys of a CLDN-2 KO mouse model are in line with this suggestion.

One of the downstream consequences of CLDN-2 down-regulation described in this study is reduced proliferation. Accumulating evidence suggests an important role for CLDN-2 as a modulator of proliferation and cell death (23, 25, 26, 71). Augmented CLDN-2 expression in some cancers correlates with poor prognosis (26, 27). Further, reduced proliferation in response to kaempferol, chrysin, luteolin, or histone deacetylase inhibitors correlated with CLDN-2 down-regulation and could be counteracted by re-expression of CLDN-2 (72, 73). A proposed mechanism described in lung and colon cancer cells is nuclear translocation of CLDN-2 and binding to the pro-proliferative transcription factor ZONAB (23, 25). Our study extends these findings by demonstrating that in tubular cells, CLDN-2 depletion slows basal and serum or TNFα-induced proliferation. We also describe a new mechanism for these effects, namely GEF-H1 and RHOA-dependent up-regulation of the CDKI P27KIP1, an inhibitor of G_1/S transition (46). Silencing experiments revealed that P27KIP1 up-regulation was necessary for reduced proliferation upon CLDN-2 depletion. The finding that RHOA had a negative effect on proliferation was somewhat unexpected, because RHOA is generally regarded as pro-proliferative. However, there is evidence for anti-proliferative actions of RHOA as well. For example, TGFβ1 induces G_2/M cell cycle arrest through RHOA-dependent inhibition of Cdc25A and C phosphatases (47). RHOA/Rho kinase can also promote apoptosis (74). Proliferation likely requires fine-tuning of RHOA activity, and both reduction and increase are detrimental. Further, the right amount of RHOA activity might be cell type–dependent.

Our finding that RHOA mediates P27KIP1 increase upon CLDN-2 silencing contrasts with some reports showing that RHOA signaling inhibits P27KIP1 (75). However, there are several mechanisms described that could cause a RHOA-dependent P27KIP1 up-regulation. For example, RHOA was shown to stabilize P27KIP1 through direct binding (46). RHOA can also reduce P27KIP1 phosphorylation via phosphatase and tensin homolog (PTEN), which is phosphorylated and activated by Rho kinase (76, 77). The PTEN is also an inhibitor of the AKT pathway, and AKT suppresses P27KIP1 transcription by inhibiting forkhead box transcription factors FoxO1/3a (78). The role of AKT in mediating GEF-H1/RHOA–dependent P27KIP1 up-regulation will require further evaluation. Irrespective of the mechanism, however, our finding suggests a possible positive feedback cycle, because P27KIP1 can also be upstream from RHOA (46).

Claudins might also be involved in feedback regulation of epithelial phenotype transition. Tight junction down-regulation is a hallmark of full-blown EMT (79), but interestingly, multiple studies now suggest, a reciprocal correlation too, namely active EMT-regulating roles for claudins. For example, Cldn-1 overexpression was shown to promote EMT, whereas Cldn-3 suppressed it (80, 81). The exact role of EMT in fibrosis is under intense debate (82). Full-blown EMT that generates myofibroblasts from tubular cells is thought not to be a major event in kidney fibrosis, although *in situ* expression of SMA in the injured epithelium has been documented. The current view, however, attributes an alternative role for the epithelium in fibrogenesis. Various harmful stimuli cause injury and interstitial inflammation, which in turn provoke the development of a profibrotic epithelial phenotype. This can be considered as partial EMT and signifies a crucial event in fibrosis (35, 83). A key feature of PEP is secretion of pro-inflammatory and profibrotic mediators, *e.g.* TGFβ1, platelet-derived growth factor, and CTGF (82, 84, 85). These in turn promote myofibroblast transition in various precursor cells (86). We and others have established that RHOA and its effector MRTF, a transcriptional coactivator of SRF (49) are master regulators of epithelial reprogramming and the ensuing PEP (35, 49). In this study we show that CLDN-2 suppresses fibrotic changes in tubular cells through its negative effects on RHOA. We found that loss of CLDN-2 activated MRTF/SRF and up-regulated its targets, the pro-fibrotic CTGF and SMA, a key myofibroblast marker (87). CLDN-2 silencing also induced RHOA-dependent up-regulation of Slug (Snail2 or Snai2) a zinc-finger 2 transcription factor belonging to the Snail family (88, 89). Because Slug is a pro-EMT transcriptional repressor of junctional proteins including E-cadherin and occludin, its up-regulation upon CLDN-2 loss is consistent with a possible positive feedback loop further promoting EMT (89). Future experiments using a broad array of EMT markers are warranted to define the effects of CLDN-2 on EMT.

Thus, our studies suggest that CLDN-2 down-regulation brought about by *e.g.* oxidative stress, drugs, or cytokines might contribute to induction of profibrotic mediator production by the tubules (83). Significantly, the major pro-fibrotic cytokine TGFβ1 does not induce EMT in resting and confluent tubular epithelial cells unless a second hit, *e.g.* disruption of the intercellular junctions is also present (53). CLDN-2 silencing by itself slightly elevates SMA levels and significantly augments the effect of TGFβ1. Thus, CLDN-2 down-regulation can provide such a second hit to prime cells to TGFβ-induced EMT. Although we found that RHOA was activated in 5-week-old CLDN-2 KO mice, we did not find evidence of increased collagen or fibronectin levels in animals up to 10 weeks old (not shown). This may be due to the young age of the animals, because fibrosis is a chronic condition. A more likely scenario is that the animals may show increased susceptibility for developing fibrosis following injury, similar to augmented injury shown by Pei *et al.* (22) in an ischemia–reperfusion model. Indeed, our observations using cell lines are consistent with a potential increase in susceptibility for fibrosis. However, this concept should be tested using fibrosis models in CLDN-2 knockout mice.

In summary, this study provides evidence that CLDN-2 is a modulator of RHOA activity, and through this propensity it can impact epithelial regeneration and fibrosis. The presence of CLDN-2 may promote proliferation upon adequate stimuli. Conversely, down-regulation of CLDN-2 in response to prolonged inflammation can support a switch from a proliferative to a pro-fibrotic state, an effect that can be crucial during epithelial regeneration but could also contribute to disease-associated fibrogenesis.

Experimental procedures

Materials and antibodies

TGFβ1 and interleukin 1β were purchased from R&D Systems (Minneapolis, MN); TNFα was from Millipore Sigma; Rhosin hydrochloride was from Tocris (Oakville, Canada). The cell-permeable Rho activator II (CN03), a version of the catalytic domain of the bacterial cytotoxic necrotizing factor toxin that activates Rho GTPase isoforms by deamidating glutamine 63, was from Cytoskeleton Inc. (Denver, CO). BSA was from BioShop (Burlington, Canada). Complete Mini Protease Inhibitor tablet and PhosSTOP Phosphatase Inhibitor tablets were from Roche Diagnostics. Rhodamine phalloidin was from Thermo Fisher Scientific/Molecular Probes. All other chemicals were from Sigma–Aldrich or BioShop.

The following antibodies against tight junction molecules were from Thermo/Invitrogen and have been validated earlier (19, 69, 90): claudin-2: monoclonal mouse antibody (catalog no. 325600) (used for Western blotting) and polyclonal rabbit antibody (catalog no. 28530) (used for immunofluorescent staining); claudin-1 (catalog no. 51-9000), ZO-1 (catalog no. 10804), claudin-7 (catalog no. 349100). Antibodies against ZO-2 (catalog no. 2847), RHOA (catalog no. 2117), GEF-H1 (55B6) (catalog no. 4076), MKL1/MRTF-A (catalog no. 14760), phosphomyosin light chain 2 (Thr-18/Ser-19) (catalog no. 3674), myosin light chain (catalog no. 3672), α-actinin (catalog no. 3431), and tubulin (catalog no. 2128) were from Cell Signaling Technology (Danvers, MA) and have been validated and used previously in Refs. 34, 38, 50, and 69. Antibodies against the HA tag (catalog no. ab137838), Ki67 (catalog no. ab15580), and GEF-H1 (pSer-885) (ab74156) were from Abcam (Cambridge, MA); GAPDH (SC-47724) was from Santa Cruz Biotechnology; P27KIP1 (catalog no. 610241) was from BD Biosciences (San Jose, CA); and α-smooth muscle actin (catalog no. A5228) was from Sigma–Aldrich. Snai2/Slug antibody was from LifeSpan Biosciences (catalog no. C353781). PCNA antibody (catalog no. bs-2006R) was from Bioss Antibodies (Woburn, MA), Active RHOA-GTP from NewEast Biosciences (catalog no. 26904) (35). Peroxidase-coupled secondary antibodies were from Jackson ImmunoResearch (West Grove, PA). Alexa Fluor 488–labeled secondary antibody was from Thermo Fisher (Waltham, MA).

Cells

LLC-PK_1, a kidney tubule epithelial cell line (male) with mostly proximal tubule characteristics from the European Collection of Animal Cell Cultures (Wiltshire, UK), was used as in our earlier studies (19, 33). Low-resistance MDCK cells, a distal tubule canine cell line (female) were from ATCC. Both cell lines were maintained in Dulbecco's modified Eagle's medium supplemented with 10% fetal bovine serum and 1% penicillin/streptomycin in an atmosphere containing 5% CO_2. Tissue culture media and reagents were from Thermo Fisher/Life Technologies. HA-tagged claudin-2 was a kind gift from Dr. Todd Alexander (91). pEGFP-C3–ZO-2 (referred to as GFP–ZO-2) was a gift from Marius Sudol (Addgene plasmid no. 27422) (92). Stable cell lines expressing HA–CLDN-2 or GFP–ZO-2 were generated by selection with G418.

Short interfering RNA

Oligonucleotides were purchased from Thermo Fisher/Dharmacon. The following porcine sequences were targeted by the siRNAs, as previously (19, 38, 50): CLDN-2 #1, CCAGAACTCTCGCGCCAAA; CLDN-2 #2, CCCTGATAGCTGGGATCAT; Cldn-1, AGTCAATGCCAGATATGAA; Cldn-7, CCAGATTGTCACAGACTTT; RHOA, AAAGCAGGTAGAGTTGGCTTT; GEF-H1, AAG CAG GGA CTG CCG GAA GCT; P27KIP1 #1 CAGCCAGCGCAAGTGGAAT; P27KIP1 #2, CAGCCAGCGCAAGTGGAAT; and MRTF-A, CCAAGGAGCTGAAGCCAAA. In MDCK the following CLDN-2 sequence was targeted: CTTCCCAGCTGGCGAACAA. The cells were transfected with 100 nM siRNA oligonucleotide using the Lipofectamine RNAiMAX transfection reagent (Thermo Fisher/Invitrogen) according to the manufacturer's instructions. Control cells were transfected with 100 nM Silencer siRNA negative control (NR siRNA) (Applied Biosystems/Ambion). Unless otherwise indicated, the experiments were performed 48 h after transfection. Down-regulation was routinely verified using Western blotting.

Western blotting

Following treatment, the cells were lysed with ice-cold lysis buffer (100 mM NaCl, 30 mM HEPES, pH 7.5, 20 mM NaF, 1 mM EGTA, 1% Triton X-100, supplemented with 1 mM Na_3VO_4, 1 mM phenylmethylsulfonyl fluoride, and protease inhibitors). For detecting phospho-myosin II (pMLC) levels, a radioimmune precipitation assay lysis buffer was used (50 mm Tris, 150 mM NaCl, 0.1% SDS, 0.5% sodium deoxycholate, 1% Triton X-100, pH 7.4) that was supplemented with protease and phosphatase inhibitors (34). Protein concentration was determined by the bicinchoninic acid assay (Thermo Fisher/Pierce Biotechnology) with BSA used as standard. SDS-PAGE and Western blotting were performed as in Ref. 19. The blots were blocked in TBS containing either 5% BSA or 5% milk and incubated with primary antibody overnight (1:1000 unless otherwise indicated). Antibody binding was visualized with peroxidase-conjugated secondary antibodies and the enhanced chemiluminescence method (kit from Bio-Rad). GAPDH (1:10000), tubulin, or α-actinin was used to demonstrate equal loading. The blots were either stripped and redeveloped or were horizontally cut following transfer, and the corresponding parts were simultaneously developed with specific antibodies. ECL signal was captured on X-ray films or with a Bio-Rad ChemiDoc Imaging System. Densitometry of films was done using a GS-800 calibrated densitometer and the Quantity One software (Bio-Rad) (69). Signal captured by ChemiDoc was quantified using Image-Lab (Bio-Rad).

Detection of MRTF molecular weight shift

Detection of MRTF molecular weight shift was carried out as in our previous study (50). Briefly, total cell lysates were run on 6% SDS gels until the 75-kDa marker reached the edge of the gel, transferred to nitrocellulose, and developed using MRTF-A antibody, with α-actinin used as loading control.

Preparation of GST fusion proteins

Preparation of GST–RBD (where RBD includes amino acids 7–89 of Rhotekin) and GST–RHOA(G17A) was described in Ref. 38. The beads were stored frozen in the presence of glycerol.

RHOA and GEF-H1 activation assay

Active (GTP-bound) RHOA and GEF-H1 were captured from cell lysates using GST–RBD or GST–RHOA(G17A), respectively (9, 38). RHOA(G17A) cannot bind nucleotide and therefore has high affinity for activated GEFs (93). Confluent LLC-PK_1 cells were treated as indicated and then lysed with ice-cold assay buffer containing 100 mM NaCl, 50 mM Tris base (pH 7.6), 20 mM NaF, 10 mM $MgCl_2$, 1% Triton X-100, 0.5% deoxycholic acid, 0.1% SDS, 1 mM Na_3VO_4, and protease inhibitors. After centrifugation, aliquots for total RHOA or GEF-H1 were removed. The remaining supernatants were incubated at 4 °C for 45 min with 20–25 μg of GST–RBD or GST–RHOA(G17A) beads, followed by extensive washing. Cell lysates (input) and captured proteins were analyzed by Western blotting and quantified by densitometry. Precipitated (active) RHOA or GEF-H1 were normalized using the corresponding input protein in the cell lysates. In the RHOA precipitation assay, the antibody regularly visualized a nonspecific band between 25 and 30 kDa. The identity of the RHOA-specific band (22 kDa) was verified using siRNA and is indicated by *black arrowheads* in the figures. Furthermore, some antibody lots also visualized a nonspecific band at ~25 kDa in the total cell lysates. To separate these, we used 15% gels and separated the 20–30-kDa area by running the gels longer.

Electric cell-substrate impedance sensing

The ECIS Ztheta system (Applied Biophysics, Troy, NY) was used to assess the effect of CLDN-2 silencing on cell growth and the development of a confluent layer (38, 44). LLC-PK_1 cells were transfected with NR or CLDN-2–specific siRNA. 24 h later the cells were trypsinized and seeded on 8W10E electrode arrays at 1.5×10^5/well. Capacitance (C) values were collected continuously at 32,000 Hz. The values were normalized to the first point representing 1.

BrdU incorporation assay

A BrdU cell proliferation assay kit (Abcam) was used, as in Ref. 38. LLC-PK_1 cells were plated on 96-well plates at 2×10^4/well in serum containing culture medium. After allowing 4 h for the cells to adhere, the medium was replaced by serum-free medium containing BrdU for overnight. BrdU incorporation was quantified using a SpectraMax Plus384 microplate spectrophotometer (Molecular Devices) at 450 nm.

Immunofluorescence microscopy

LLC-PK_1 cells grown on coverslips were fixed with 4% paraformaldehyde or ice-cold methanol (for CLDN-2), washed, and blocked with 3% BSA in PBS. Following permeabilization, coverslips were incubated with primary antibody (1:100, 1 h), followed by washes and incubation with Alexa Fluor 488–labeled secondary antibody (1:1000). The nuclei were counterstained with DAPI. The slides were viewed using a WaveFX spinning-disk confocal microscope (Quorum Technologies, Guelph, Canada) with an ORCA-flash4.0 digital camera with Gen II sCMOS image sensor. Maximum intensity projection pictures were generated from Z-stack using the Metamorph software. For staining F-actin, fixed and permeabilized cells were incubated with rhodamine phalloidin (Invitrogen). To visualize stress fibers, maximum intensity projection images from stacks of the bottom 4 μm of the cells (12–15 slices) were obtained.

Active RHOA in kidney tissues

Active RHOA in kidney tissues was labeled as in Ref. 35. Briefly, paraffin-embedded kidney sections were stained with anti-RHOA-GTP as in Ref. 35. Briefly, after deparaffinization, slides underwent heat-induced antigen retrieval, followed by blocking with DAKO serum-free protein blocking reagent, and were exposed to active RHOA antibody (New East Bioscience catalog no. 26904) (1:500) at 4 °C, overnight. After washing, the samples were incubated with Alexa Fluor 555–labeled anti-mouse antibody (Invitrogen) (1:500) (1 h). Images were captured and scanned using Zeiss Axio Observer microscope and analyzed by the Zen Blue software. Background staining was determined and subtracted using parallel staining with secondary antibody only. Representative images are shown from each condition.

Unilateral ureteric obstruction

All animal studies were carried out according to a protocol approved by the animal care committee of the St. Michael's Hospital. Male C57BL/6 mice (6–8 weeks old, from Jackson Laboratory (Bar Harbor, ME)), underwent surgery as described previously (34). Briefly, the left ureter was ligated. Three- or seven-days after surgery, the mice were sacrificed, and the left kidneys were harvested. Half of the kidney was snap-frozen in liquid nitrogen, and the other half was fixed and embedded in paraffin or frozen fresh in OCT medium. The samples were stored at −80 °C until further processing.

CLDN-2 KO mice

CLDN-2 KO mice were acquired from the Mutant Mouse Resource and Research Centres at UC Davis. The strain is referred to as B6;129S5-*Cldn2*^{tm1Lex}/Mmucd and has been described before (21, 22). This strain was backcrossed onto WT FVB/N mice (Jackson Laboratories) for >5 generations. Standard pelleted chow (PicoLab Rodent Diet 5053: 21% (w/w) protein, 5.0% (w/w) fat, 0.81% (w/w) Ca^{2+}, and 2.2 IU/g vitamin D_3) and drinking water were available *ad libitum*. Genotyping was performed using primers 5′-CAGGCTCCGAAGATACTTC and 5′-GTAGAAGTCCCGAAGGATG for the WT reaction and 5′-CAGGCTCCGAAGATACTTC and 5′-CCCTAGGA-

ATGCTCGTCAAGA for the knockout reaction. At 5 weeks WT and claudin-2 KO mice were euthanized, and kidney tissue was either snap frozen as previously (94) or fixed in formaldehyde and embedded in paraffin for processing for immunofluorescent staining. All animal experiments were approved by the Animal Care and Use Committee for Health Science of the University of Alberta (protocol no. 213).

Immunohistochemistry and quantification

Staining and quantification of paraffin-embedded kidney sections was performed as in (35), using P27KIP1 antibody. Standard immunohistochemistry protocol was used, with horseradish peroxidase-labeled secondary antibody and a 3,3′-diaminobenzidine (DAB)+ substrate chromogen system from Agilent, Dako (Mississauga, Canada). Histological slides were viewed by an Olympus BX50 microscope driven by the Cellsense software. The slides were analyzed using the Fiji software. To quantify the DAB-positive signal in each image, color deconvolution was applied using the Fiji software, followed by thresholding. The number of positive pixels was then expressed as fold change compared with sham.

RT-PCR for mRNA analysis

RNA was extracted using the RNeasy kit (Qiagen), and cDNA was synthesized using iScript reverse transcriptase (Bio-Rad). SYBR green-based real-time PCR was performed as in Ref. 19. Primer pairs designed against the corresponding mouse sequences were as follows: Claudin-2, 5′-CCCAGGCCATGATGGTGA-3′ and 5′-TCATGCCCACCACAGAGATAAT-3′; SGLT-2, 5′-CATAAAGTCGAGGGTGTT-3′ and 5′-GGAAGTGACAACCAATCA-3′(95); Claudin-1, 5′-CTGGAAGATGATGAGGTGCAGAAGA-3′ and 5′-CCACTAATGTCGCCAGACCTGAA-3′; Claudin-7, 5′-CCTGGTGTTGGGCTTCTTAGC-3′ and 5′-CCCACAGCGTGTGCACTTC-3′; and GAPDH, 5′-GCAAAGTGGACATGGTCGCCATCA-3′ and 5′-AGCTTCCCATTCTCAGCCTTGACT-3′ (19).

The following primers were used to detect pig mRNA: claudin-2, 5′-GCACTGGCATCACCCAGTGT-3′ and 5′-GATGATACAGGCCAACGAGG-3′; claudin-1, F, 5′-TTCTGGGAGGTGCCCTACTT-3′ and 5′-TGGATAGGGCCTTGGTGTTG-3′; Claudin-7, 5′-ACTTAAAATTCGCCCACCCG-3′ and 5′-TGACGCAGTCCATCCATAGC-3′; and GAPDH, 5′-GCAAAGTGGACATGGTCGCCATCA-3′ and 5′-AGCTTCCCATTCTCAGCCTTGACT-3′.

Laser capture microdissection

LCM was performed as earlier (34). Mouse kidneys from sham and UUO (7 days) animals were embedded in Tissue-Tek OCT medium, frozen in liquid nitrogen, and stored at −80 °C. For processing, the tissues were sectioned at 2–5 μm, mounted on glass slides, and stained using a rapid hematoxylin and eosin–staining protocol (Mayer's hematoxylin solution and alcoholic eosin Y solution from Sigma). LCM was carried out using the PixCell II laser capture microdissection system and CapSure LCM Caps (Arcturus Mountain View, CA), with the following parameters: spot size, 7.5 μm; power, 65 milliwatt; and duration, 650 μs. A total of 100–200 target tubules and interstitial areas were captured for each sample. Total RNA from LCM-captured samples was isolated using the RNeasy micro RNA isolation kit (Qiagen) and reverse-transcribed using a Sensiscript reverse transcription kit (Qiagen) with oligo(dT) primer. PCR was performed using the iproof high-fidelity PCR kit (Bio-Rad). The following primers were used to evaluate tubular markers: Tamm–Horsfall protein (THP) (sense, 5′-TCA-GCC-TGA-AGA-CCT-CCC-TA-3′; antisense, 5′-TGT-GGC-ATA-GCA-GTT-GGT-CA-3′); basic amino acid transporter (BAT) (sense, 5′-ACG-TCT-TCC-TCG-TGG-TTC-TG-3′; antisense, 5′-GCC-ATC-TCT-TAG-GGA-GCT-T-3′), and GAPDH (sense, 5′-ACC-ACA-GTC-CAT-GCC-ATC-AC-3′; antisense, 5′-CAC-CAC-CCT-GTT-GCT-GTA-GCC-3′).

Luciferase reporter assay

Luciferase reporter assay was performed as previously (50, 69), with some modifications. The cells were plated on 24-well plates and at ~60% confluence transfected using jetPrime (Polyplus transfection, New York, NY). The transfection mix contained 0.5 μg/well pGL3–3DA-luc reporter plasmid (Firefly luciferase gene under the control of a CArG box triplet) (50, 96) along with the normalizing vector enhancer-less *Renilla* luciferase, pRL-TK (Promega) (0.125 μg/well), and, where indicated NR or CLDN-2–specific siRNA. In some experiments promoter-transfected cells were treated overnight with 30 μM Rhosin. 24 h after transfection, the cells were lysed, and luciferase activity was measured using the Dual-Luciferase reporter assay system kit (Promega) and a Berthold Lumat 9507 luminometer according to the manufacturers' instructions. Treatments were done in duplicate, and the experiments were repeated at least three times. For each sample firefly luciferase activity corresponding to the 3DA promoter construct was normalized to the *Renilla* luciferase activity. The results were expressed as fold changes compared with the mean firefly/*Renilla* ratio of the untreated controls taken as a unity.

Statistical analysis

All blots and immunofluorescent pictures are representatives of at least three similar experiments. The data are presented as means ± S.D. of the number of experiments indicated (n). Statistical significance was assessed by one-way analysis of variance performed using the GraphPad Prism software. Unless otherwise indicated, Tukey's post hoc test was used. For comparison of two conditions, Student's t test (unpaired, equal variance) was performed.

Author contributions—Q. D., Y. S., R. R., S. V., and P. S. formal analysis; Q. D., Y. S., R. R., S. V., J. X., S. A., M. D., and P. S. investigation; Q. D., Y. S., and P. S. methodology; R. R., S. V., and A. K. writing-review and editing; S. V., M. D., and K. S. data curation; W.P. and R.T.A. resources; A. K. and K. S. conceptualization; A. K. and K. S. supervision; A. K. and K. S. funding acquisition; K. S. writing-original draft; K. S. project administration.

Acknowledgments—We thank the Keenan Research Center core facility managers for assistance.

References

1. Van Itallie, C. M., and Anderson, J. M. (2014) Architecture of tight junctions and principles of molecular composition. *Semin. Cell Dev. Biol.* **36,** 157–165 CrossRef Medline
2. Yano, T., Kanoh, H., Tamura, A., and Tsukita, S. (2017) Apical cytoskeletons and junctional complexes as a combined system in epithelial cell sheets. *Ann. N.Y. Acad. Sci.* **1405,** 32–43 CrossRef Medline
3. Ivanov, A. I. (2008) Actin motors that drive formation and disassembly of epithelial apical junctions. *Front. Biosci.* **13,** 6662–6681 Medline
4. Citi, S., Guerrera, D., Spadaro, D., and Shah, J. (2014) Epithelial junctions and Rho family GTPases: the zonular signalosome. *Small GTPases* **5,** 1–15
5. Cherfils, J., and Zeghouf, M. (2013) Regulation of small GTPases by GEFs, GAPs, and GDIs. *Physiol. Rev.* **93,** 269–309 CrossRef Medline
6. Guillemot, L., Paschoud, S., Jond, L., Foglia, A., and Citi, S. (2008) Paracingulin regulates the activity of Rac1 and RHOA GTPases by recruiting Tiam1 and GEF-H1 to epithelial junctions. *Mol. Biol. Cell* **19,** 4442–4453 CrossRef Medline
7. Aijaz, S., D'Atri, F., Citi, S., Balda, M. S., and Matter, K. (2005) Binding of GEF-H1 to the tight junction-associated adaptor cingulin results in inhibition of Rho signaling and G_1/S phase transition. *Dev. Cell* **8,** 777–786 CrossRef Medline
8. Raya-Sandino, A., Castillo-Kauil, A., Domínguez-Calderón, A., Alarcón, L., Flores-Benitez, D., Cuellar-Perez, F., López-Bayghen, B., Chávez-Munguía, B., Vázquez-Prado, J., and González-Mariscal, L. (2017) Zonula occludens-2 regulates Rho proteins activity and the development of epithelial cytoarchitecture and barrier function. *Biochim. Biophys. Acta Mol. Cell Res.* **1864,** 1714–1733 CrossRef Medline
9. Kakiashvili, E., Speight, P., Waheed, F., Seth, R., Lodyga, M., Tanimura, S., Kohno, M., Rotstein, O. D., Kapus, A., and Szászi, K. (2009) GEF-H1 mediates tumor necrosis factor-α-induced Rho activation and myosin phosphorylation: role in the regulation of tubular paracellular permeability. *J. Biol. Chem.* **284,** 11454–11466 CrossRef Medline
10. Fromm, M., Piontek, J., Rosenthal, R., Günzel, D., and Krug, S. M. (2017) Tight junctions of the proximal tubule and their channel proteins. *Pflugers Arch.* **469,** 877–887 CrossRef Medline
11. Guillemot, L., Paschoud, S., Pulimeno, P., Foglia, A., and Citi, S. (2008) The cytoplasmic plaque of tight junctions: a scaffolding and signalling center. *Biochim. Biophys. Acta* **1778,** 601–613 CrossRef Medline
12. Singh, A. B., Uppada, S. B., and Dhawan, P. (2017) Claudin proteins, outside-in signaling, and carcinogenesis. *Pflugers Arch.* **469,** 69–75 CrossRef Medline
13. Weber, C. R., Liang, G. H., Wang, Y., Das, S., Shen, L., Yu, A. S., Nelson, D. J., and Turner, J. R. (2015) Claudin-2–dependent paracellular channels are dynamically gated. *Elife* **4,** e09906 CrossRef Medline
14. Rosenthal, R., Gunzel, D., Krug, S. M., Schulzke, J. D., Fromm, M., and Yu, A. S. (2017) Claudin-2-mediated cation and water transport share a common pore. *Acta Physiol.* (*Oxf.*) **219,** 521–536 CrossRef Medline
15. Furuse, M., Furuse, K., Sasaki, H., and Tsukita, S. (2001) Conversion of zonulae occludentes from tight to leaky strand type by introducing claudin-2 into Madin–Darby canine kidney I cells. *J. Cell Biol.* **153,** 263–272 CrossRef Medline
16. Amasheh, S., Meiri, N., Gitter, A. H., Schöneberg, T., Mankertz, J., Schulzke, J. D., and Fromm, M. (2002) Claudin-2 expression induces cation-selective channels in tight junctions of epithelial cells. *J. Cell Sci.* **115,** 4969–4976 CrossRef Medline
17. Hou, J., Gomes, A. S., Paul, D. L., and Goodenough, D. A. (2006) Study of claudin function by RNA interference. *J. Biol. Chem.* **281,** 36117–36123 CrossRef Medline
18. Tokuda, S., and Furuse, M. (2015) Claudin-2 knockout by TALEN-mediated gene targeting in MDCK cells: claudin-2 independently determines the leaky property of tight junctions in MDCK cells. *PLoS One* **10,** e0119869 CrossRef Medline
19. Amoozadeh, Y., Dan, Q., Xiao, J., Waheed, F., and Szászi, K. (2015) Tumor necrosis factor-α induces a biphasic change in claudin-2 expression in tubular epithelial cells: role in barrier functions. *Am. J. Physiol. Cell Physiol.* **309,** C38–C50 CrossRef Medline
20. Muto, S., Hata, M., Taniguchi, J., Tsuruoka, S., Moriwaki, K., Saitou, M., Furuse, K., Sasaki, H., Fujimura, A., Imai, M., Kusano, E., Tsukita, S., and Furuse, M. (2010) Claudin-2-deficient mice are defective in the leaky and cation-selective paracellular permeability properties of renal proximal tubules. *Proc. Natl. Acad. Sci. U.S.A.* **107,** 8011–8016 CrossRef Medline
21. Schnermann, J., Huang, Y., and Mizel, D. (2013) Fluid reabsorption in proximal convoluted tubules of mice with gene deletions of claudin-2 and/or aquaporin1. *Am. J. Physiol. Renal Physiol.* **305,** F1352–F1364 CrossRef Medline
22. Pei, L., Solis, G., Nguyen, M. T., Kamat, N., Magenheimer, L., Zhuo, M., Li, J., Curry, J., McDonough, A. A., Fields, T. A., Welch, W. J., and Yu, A. S. (2016) Paracellular epithelial sodium transport maximizes energy efficiency in the kidney. *J. Clin. Invest.* **126,** 2509–2518 CrossRef Medline
23. Ikari, A., Watanabe, R., Sato, T., Taga, S., Shimobaba, S., Yamaguchi, M., Yamazaki, Y., Endo, S., Matsunaga, T., and Sugatani, J. (2014) Nuclear distribution of claudin-2 increases cell proliferation in human lung adenocarcinoma cells. *Biochim. Biophys. Acta* **1843,** 2079–2088 CrossRef Medline
24. Ikari, A., Sato, T., Takiguchi, A., Atomi, K., Yamazaki, Y., and Sugatani, J. (2011) Claudin-2 knockdown decreases matrix metalloproteinase-9 activity and cell migration via suppression of nuclear Sp1 in A549 cells. *Life Sci.* **88,** 628–633 CrossRef Medline
25. Buchert, M., Papin, M., Bonnans, C., Darido, C., Raye, W. S., Garambois, V., Pélegrin, A., Bourgaux, J. F., Pannequin, J., Joubert, D., and Hollande, F. (2010) Symplekin promotes tumorigenicity by up-regulating claudin-2 expression. *Proc. Natl. Acad. Sci. U.S.A.* **107,** 2628–2633 CrossRef Medline
26. Paquet-Fifield, S., Koh, S. L., Cheng, L., Beyit, L. M., Shembrey, C., Mølck, C., Behrenbruch, C., Papin, M., Gironella, M., Guelfi, S., Nasr, R., Grillet, F., Prudhomme, M., Bourgaux, J. F., Castells, A., *et al.* (2018) Tight junction protein claudin-2 promotes self-renewal of human colorectal cancer stem-like cells. *Cancer Res.* **78,** 2925–2938 CrossRef Medline
27. Kimbung, S., Kovács, A., Bendahl, P. O., Malmström, P., Fernö, M., Hatschek, T., and Hedenfalk, I. (2014) Claudin-2 is an independent negative prognostic factor in breast cancer and specifically predicts early liver recurrences. *Mol. Oncol.* **8,** 119–128 CrossRef Medline
28. Szaszi, K., and Amoozadeh, Y. (2014) New insights into functions, regulation, and pathological roles of tight junctions in kidney tubular epithelium. *Int. Rev. Cell Mol. Biol.* **308,** 205–271 CrossRef Medline
29. Mankertz, J., and Schulzke, J. D. (2007) Altered permeability in inflammatory bowel disease: pathophysiology and clinical implications. *Curr. Opin. Gastroenterol.* **23,** 379–383 CrossRef Medline
30. Balkovetz, D. F., Chumley, P., and Amlal, H. (2009) Downregulation of claudin-2 expression in renal epithelial cells by metabolic acidosis. *Am. J. Physiol. Renal Physiol.* **297,** F604–F611 CrossRef Medline
31. Ikari, A., Takiguchi, A., Atomi, K., Sato, T., and Sugatani, J. (2011) Decrease in claudin-2 expression enhances cell migration in renal epithelial Madin–Darby canine kidney cells. *J. Cell Physiol.* **226,** 1471–1478 CrossRef Medline
32. Gonzalez, J. E., DiGeronimo, R. J., Arthur, D. E., and King, J. M. (2009) Remodeling of the tight junction during recovery from exposure to hydrogen peroxide in kidney epithelial cells. *Free Radic. Biol. Med.* **47,** 1561–1569 CrossRef Medline
33. Martin-Martin, N., Dan, Q., Amoozadeh, Y., Waheed, F., McMorrow, T., Ryan, M. P., and Szászi, K. (2012) RHOA and Rho kinase mediate cyclosporine A and sirolimus-induced barrier tightening in renal proximal tubular cells. *Int. J. Biochem. Cell Biol.* **44,** 178–188 CrossRef Medline
34. Rozycki, M., Bialik, J. F., Speight, P., Dan, Q., Knudsen, T. E., Szeto, S. G., Yuen, D. A., Szászi, K., Pedersen, S. F., and Kapus, A. (2016) Myocardin-related transcription factor regulates Nox4 protein expression: linking cytoskeletal organization to redox state. *J. Biol. Chem.* **291,** 227–243 CrossRef Medline
35. Bialik, J. F., Ding, M., Speight, P., Dan, Q., Miranda, M. Z., Di Ciano-Oliveira, C., Kofler, M. M., Rotstein, O. D., Pedersen, S. F., Szászi, K., and Kapus, A. (2019) Profibrotic epithelial phenotype: a central role for MRTF and TAZ. *Sci. Rep.* **9,** 4323 CrossRef Medline
36. Klahr, S., and Morrissey, J. (2002) Obstructive nephropathy and renal fibrosis. *Am. J. Physiol. Renal Physiol.* **283,** F861–F875 CrossRef Medline

37. Szászi, K., Sirokmány, G., Di Ciano-Oliveira, C., Rotstein, O. D., and Kapus, A. (2005) Depolarization induces Rho-Rho kinase-mediated myosin light chain phosphorylation in kidney tubular cells. *Am. J. Physiol. Cell Physiol.* **289,** C673–C685 CrossRef Medline
38. Waheed, F., Dan, Q., Amoozadeh, Y., Zhang, Y., Tanimura, S., Speight, P., Kapus, A., and Szászi, K. (2013) Central role of the exchange factor GEF-H1 in TNF-α–induced sequential activation of Rac, ADAM17/TACE, and RHOA in tubular epithelial cells. *Mol. Biol. Cell* **24,** 1068–1082 CrossRef Medline
39. Birkenfeld, J., Nalbant, P., Yoon, S. H., and Bokoch, G. M. (2008) Cellular functions of GEF-H1, a microtubule-regulated Rho-GEF: is altered GEF-H1 activity a crucial determinant of disease pathogenesis? *Trends Cell Biol.* **18,** 210–219 CrossRef Medline
40. Benais-Pont, G., Punn, A., Flores-Maldonado, C., Eckert, J., Raposo, G., Fleming, T. P., Cereijido, M., Balda, M. S., and Matter, K. (2003) Identification of a tight junction-associated guanine nucleotide exchange factor that activates Rho and regulates paracellular permeability. *J. Cell Biol.* **160,** 729–740 CrossRef Medline
41. Terry, S. J., Zihni, C., Elbediwy, A., Vitiello, E., Leefa Chong San, I. V., Balda, M. S., and Matter, K. (2011) Spatially restricted activation of RHOA signalling at epithelial junctions by p114RhoGEF drives junction formation and morphogenesis. *Nat. Cell Biol.* **13,** 159–166 CrossRef Medline
42. Zenke, F. T., Krendel, M., DerMardirossian, C., King, C. C., Bohl, B. P., and Bokoch, G. M. (2004) p21-activated kinase 1 phosphorylates and regulates 14-3-3 binding to GEF-H1, a microtubule-localized Rho exchange factor. *J. Biol. Chem.* **279,** 18392–18400 CrossRef Medline
43. Hong, J., Kandasamy, K., Marimuthu, M., Choi, C. S., and Kim, S. (2011) Electrical cell-substrate impedance sensing as a non-invasive tool for cancer cell study. *Analyst* **136,** 237–245 CrossRef Medline
44. Wegener, J., Keese, C. R., and Giaever, I. (2000) Electric cell-substrate impedance sensing (ECIS) as a noninvasive means to monitor the kinetics of cell spreading to artificial surfaces. *Exp. Cell Res.* **259,** 158–166 CrossRef Medline
45. Kakiashvili, E., Dan, Q., Vandermeer, M., Zhang, Y., Waheed, F., Pham, M., and Szászi, K. (2011) The epidermal growth factor receptor mediates tumor necrosis factor-α–induced activation of the ERK/GEF-H1/RHOA pathway in tubular epithelium. *J. Biol. Chem.* **286,** 9268–9279 CrossRef Medline
46. Abbastabar, M., Kheyrollah, M., Azizian, K., Bagherlou, N., Tehrani, S. S., Maniati, M., and Karimian, A. (2018) Multiple functions of p27 in cell cycle, apoptosis, epigenetic modification and transcriptional regulation for the control of cell growth: A double-edged sword protein. *DNA Repair (Amst.)* **69,** 63–72 CrossRef Medline
47. Bhowmick, N. A., Ghiassi, M., Aakre, M., Brown, K., Singh, V., and Moses, H. L. (2003) TGF-β–induced RHOA and p160ROCK activation is involved in the inhibition of Cdc25A with resultant cell-cycle arrest. *Proc. Natl. Acad. Sci. U.S.A.* **100,** 15548–15553 CrossRef Medline
48. Masszi, A., Di Ciano, C., Sirokmány, G., Arthur, W. T., Rotstein, O. D., Wang, J., McCulloch, C. A., Rosivall, L., Mucsi, I., and Kapus, A. (2003) Central role for Rho in TGF-β1–induced α-smooth muscle actin expression during epithelial-mesenchymal transition. *Am. J. Physiol. Renal Physiol.* **284,** F911–F924 CrossRef Medline
49. Gasparics, Á., and Sebe, A. (2018) MRTFs: master regulators of EMT. *Dev. Dyn.* **247,** 396–404 CrossRef Medline
50. Miranda, M. Z., Bialik, J. F., Speight, P., Dan, Q., Yeung, T., Szászi, K., Pedersen, S. F., and Kapus, A. (2017) TGF-β1 regulates the expression and transcriptional activity of TAZ protein via a Smad3-independent, myocardin-related transcription factor-mediated mechanism. *J. Biol. Chem.* **292,** 14902–14920 CrossRef Medline
51. Panayiotou, R., Miralles, F., Pawlowski, R., Diring, J., Flynn, H. R., Skehel, M., and Treisman, R. (2016) Phosphorylation acts positively and negatively to regulate MRTF-A subcellular localisation and activity. *Elife* **5,** e15460 CrossRef Medline
52. Haak, A. J., Tsou, P. S., Amin, M. A., Ruth, J. H., Campbell, P., Fox, D. A., Khanna, D., Larsen, S. D., and Neubig, R. R. (2014) Targeting the myofibroblast genetic switch: inhibitors of myocardin-related transcription factor/serum response factor-regulated gene transcription prevent fibrosis in a murine model of skin injury. *J. Pharmacol. Exp. Ther.* **349,** 480–486 CrossRef Medline
53. Fan, L., Sebe, A., Péterfi, Z., Masszi, A., Thirone, A. C., Rotstein, O. D., Nakano, H., McCulloch, C. A., Szászi, K., Mucsi, I., and Kapus, A. (2007) Cell contact-dependent regulation of epithelial-myofibroblast transition via the rho-rho kinase-phospho-myosin pathway. *Mol. Biol. Cell* **18,** 1083–1097 CrossRef Medline
54. Masszi, A., Fan, L., Rosivall, L., McCulloch, C. A., Rotstein, O. D., Mucsi, I., and Kapus, A. (2004) Integrity of cell-cell contacts is a critical regulator of TGF-β1–induced epithelial-to-myofibroblast transition: role for β-catenin. *Am. J. Pathol.* **165,** 1955–1967 CrossRef Medline
55. Barmeyer, C., Fromm, M., and Schulzke, J. D. (2017) Active and passive involvement of claudins in the pathophysiology of intestinal inflammatory diseases. *Pflugers Arch.* **469,** 15–26 CrossRef Medline
56. García-Hernández, V., Flores-Maldonado, C., Rincon-Heredia, R., Verdejo-Torres, O., Bonilla-Delgado, J., Meneses-Morales, I., Gariglio, P., and Contreras, R. G. (2015) EGF regulates claudin-2 and -4 expression through Src and STAT3 in MDCK cells. *J. Cell Physiol.* **230,** 105–115 CrossRef Medline
57. Kawkitinarong, K., Linz-McGillem, L., Birukov, K. G., and Garcia, J. G. (2004) Differential regulation of human lung epithelial and endothelial barrier function by thrombin. *Am. J. Respir. Cell Mol. Biol.* **31,** 517–527 CrossRef Medline
58. Zhang, X. E., Adderley, S. P., and Breslin, J. W. (2016) Activation of RHOA, but not Rac1, mediates early stages of S1P-induced endothelial barrier enhancement. *PLoS One* **11,** e0155490 CrossRef Medline
59. Garcia, J. G., Liu, F., Verin, A. D., Birukova, A., Dechert, M. A., Gerthoffer, W. T., Bamberg, J. R., and English, D. (2001) Sphingosine 1-phosphate promotes endothelial cell barrier integrity by Edg-dependent cytoskeletal rearrangement. *J. Clin. Invest.* **108,** 689–701 CrossRef Medline
60. Xu, M., Waters, C. L., Hu, C., Wysolmerski, R. B., Vincent, P. A., and Minnear, F. L. (2007) Sphingosine 1-phosphate rapidly increases endothelial barrier function independently of VE-cadherin but requires cell spreading and Rho kinase. *Am. J. Physiol. Cell Physiol.* **293,** C1309–C1318 CrossRef Medline
61. Szulcek, R., Beckers, C. M., Hodzic, J., de Wit, J., Chen, Z., Grob, T., Musters, R. J., Minshall, R. D., van Hinsbergh, V. W., and van Nieuw Amerongen, G. P. (2013) Localized RHOA GTPase activity regulates dynamics of endothelial monolayer integrity. *Cardiovasc. Res.* **99,** 471–482 CrossRef Medline
62. Walsh, S. V., Hopkins, A. M., Chen, J., Narumiya, S., Parkos, C. A., and Nusrat, A. (2001) Rho kinase regulates tight junction function and is necessary for tight junction assembly in polarized intestinal epithelia. *Gastroenterology* **121,** 566–579 CrossRef Medline
63. Itoh, M., Tsukita, S., Yamazaki, Y., and Sugimoto, H. (2012) Rho GTP exchange factor ARHGEF11 regulates the integrity of epithelial junctions by connecting ZO-1 and RHOA-myosin II signaling. *Proc. Natl. Acad. Sci. U.S.A.* **109,** 9905–9910 CrossRef Medline
64. Waheed, F., Speight, P., Dan, Q., Garcia-Mata, R., and Szaszi, K. (2012) Affinity precipitation of active Rho-GEFs using a GST-tagged mutant Rho protein (GST–RHOA(G17A)) from epithelial cell lysates. *J. Vis. Exp.* 3932
65. Birkenfeld, J., Nalbant, P., Bohl, B. P., Pertz, O., Hahn, K. M., and Bokoch, G. M. (2007) GEF-H1 modulates localized RHOA activation during cytokinesis under the control of mitotic kinases. *Dev. Cell* **12,** 699–712 CrossRef Medline
66. Guilluy, C., Swaminathan, V., Garcia-Mata, R., O'Brien, E. T., Superfine, R., and Burridge, K. (2011) The Rho GEFs LARG and GEF-H1 regulate the mechanical response to force on integrins. *Nat. Cell Biol.* **13,** 722–727 CrossRef Medline
67. Tsapara, A., Luthert, P., Greenwood, J., Hill, C. S., Matter, K., and Balda, M. S. (2010) The RhoA activator GEF-H1/Lfc is a TGF-β target gene and effector that regulates α-smooth muscle actin expression and cell migration. *Mol. Biol. Cell* **21,** 860–870 CrossRef Medline
68. Pathak, R., Delorme-Walker, V. D., Howell, M. C., Anselmo, A. N., White, M. A., Bokoch, G. M., and Dermardirossian, C. (2012) The microtubule-associated Rho activating factor GEF-H1 interacts with exocyst complex to regulate vesicle traffic. *Dev. Cell* **23,** 397–411 CrossRef Medline

69. Amoozadeh, Y., Anwer, S., Dan, Q., Venugopal, S., Shi, Y., Branchard, E., Liedtke, E., Ailenberg, M., Rotstein, O. D., Kapus, A., and Szászi, K. (2018) Cell confluence regulates claudin-2 expression: possible role for ZO-1 and Rac. *Am. J. Physiol. Cell Physiol.* **314,** C366–C378 CrossRef Medline
70. Yano, T., Matsui, T., Tamura, A., Uji, M., and Tsukita, S. (2013) The association of microtubules with tight junctions is promoted by cingulin phosphorylation by AMPK. *J. Cell Biol.* **203,** 605–614 CrossRef Medline
71. Dhawan, P., Ahmad, R., Chaturvedi, R., Smith, J. J., Midha, R., Mittal, M. K., Krishnan, M., Chen, X., Eschrich, S., Yeatman, T. J., Harris, R. C., Washington, M. K., Wilson, K. T., Beauchamp, R. D., and Singh, A. B. (2011) Claudin-2 expression increases tumorigenicity of colon cancer cells: role of epidermal growth factor receptor activation. *Oncogene* **30,** 3234–3247 CrossRef Medline
72. Sonoki, H., Tanimae, A., Endo, S., Matsunaga, T., Furuta, T., Ichihara, K., and Ikari, A. (2017) Kaempherol and luteolin decrease claudin-2 expression mediated by inhibition of STAT3 in lung adenocarcinoma A549 cells. *Nutrients* **9,** E597 Medline
73. Hichino, A., Okamoto, M., Taga, S., Akizuki, R., Endo, S., Matsunaga, T., and Ikari, A. (2017) Down-regulation of Claudin-2 expression and proliferation by epigenetic inhibitors in human lung adenocarcinoma A549 cells. *J. Biol. Chem.* **292,** 2411–2421 CrossRef Medline
74. Shi, J., and Wei, L. (2007) Rho kinase in the regulation of cell death and survival. *Arch. Immunol. Ther. Exp.* (*Warsz.*) **55,** 61–75 CrossRef Medline
75. Croft, D. R., and Olson, M. F. (2006) The Rho GTPase effector ROCK regulates cyclin A, cyclin D1, and P27KIP1 levels by distinct mechanisms. *Mol. Cell Biol.* **26,** 4612–4627 CrossRef Medline
76. Hsu, Y. H., Chang, C. C., Yang, N. J., Lee, Y. H., and Juan, S. H. (2014) RhoA-mediated inhibition of vascular endothelial cell mobility: positive feedback through reduced cytosolic p21 and p27. *J. Cell Physiol.* **229,** 1455–1465 CrossRef Medline
77. Krauszman, A., Mak, T. W., Szaszi, K., and Kuebler, W. M. (2017) Role of phosphatase and tensin homolog (PTEN) in hypoxic pulmonary vasoconstriction. *Cardiovasc. Res.* **113,** 869–878 CrossRef Medline
78. Manning, B. D., and Toker, A. (2017) AKT/PKB signaling: navigating the network. *Cell* **169,** 381–405 CrossRef Medline
79. Kalluri, R., and Weinberg, R. A. (2009) The basics of epithelial-mesenchymal transition. *J. Clin. Invest.* **119,** 1420–1428 CrossRef Medline
80. Stebbing, J., Filipović, A., and Giamas, G. (2013) Claudin-1 as a promoter of EMT in hepatocellular carcinoma. *Oncogene* **32,** 4871–4872 CrossRef Medline
81. Che, J., Yue, D., Zhang, B., Zhang, H., Huo, Y., Gao, L., Zhen, H., Yang, Y., and Cao, B. (2018) Claudin-3 inhibits lung squamous cell carcinoma cell epithelial-mesenchymal transition and invasion via suppression of the Wnt/β-catenin signaling pathway. *Int. J. Med. Sci.* **15,** 339–351 CrossRef Medline
82. Quaggin, S. E., and Kapus, A. (2011) Scar wars: mapping the fate of epithelial-mesenchymal-myofibroblast transition. *Kidney Int.* **80,** 41–50 CrossRef Medline
83. Liu, B. C., Tang, T. T., Lv, L. L., and Lan, H. Y. (2018) Renal tubule injury: a driving force toward chronic kidney disease. *Kidney Int.* **93,** 568–579 CrossRef Medline
84. Rodríguez-Iturbe, B., and García García, G. (2010) The role of tubulointerstitial inflammation in the progression of chronic renal failure. *Nephron Clin. Pract.* **116,** c81–c88 CrossRef Medline
85. Masszi, A., and Kapus, A. (2011) Smaddening complexity: the role of Smad3 in epithelial-myofibroblast transition. *Cells Tissues Organs* **193,** 41–52 CrossRef Medline
86. Ferenbach, D. A., and Bonventre, J. V. (2015) Mechanisms of maladaptive repair after AKI leading to accelerated kidney ageing and CKD. *Nat. Rev. Nephrol.* **11,** 264–276 CrossRef Medline
87. Masszi, A., Speight, P., Charbonney, E., Lodyga, M., Nakano, H., Szászi, K., and Kapus, A. (2010) Fate-determining mechanisms in epithelial-myofibroblast transition: major inhibitory role for Smad3. *J. Cell Biol.* **188,** 383–399 CrossRef Medline
88. Wang, Y., Shi, J., Chai, K., Ying, X., and Zhou, B. P. (2013) The role of Snail in EMT and tumorigenesis. *Curr. Cancer Drug Targets* **13,** 963–972 CrossRef Medline
89. Boutet, A., De Frutos, C. A., Maxwell, P. H., Mayol, M. J., Romero, J., and Nieto, M. A. (2006) Snail activation disrupts tissue homeostasis and induces fibrosis in the adult kidney. *EMBO J.* **25,** 5603–5613 CrossRef Medline
90. Amoozadeh, Y., Dan, Q., Anwer, S., Huang, H. H., Barbieri, V., Waheed, F., Maishan, M., and Szászi, K. (2017) Tumor necrosis factor-α increases Claudin-1, 4, and 7 expression in tubular cells: role in permeability changes. *J. Cell Physiol.* **232,** 2210–2220 CrossRef Medline
91. Borovac, J., Barker, R. S., Rievaj, J., Rasmussen, A., Pan, W., Wevrick, R., and Alexander, R. T. (2012) Claudin-4 forms a paracellular barrier, revealing the interdependence of claudin expression in the loose epithelial cell culture model opossum kidney cells. *Am. J. Physiol. Cell Physiol.* **303,** C1278–C1291 CrossRef Medline
92. Oka, T., Remue, E., Meerschaert, K., Vanloo, B., Boucherie, C., Gfeller, D., Bader, G. D., Sidhu, S. S., Vandekerckhove, J., Gettemans, J., and Sudol, M. (2010) Functional complexes between YAP2 and ZO-2 are PDZ domain-dependent, and regulate YAP2 nuclear localization and signalling. *Biochem. J.* **432,** 461–472 CrossRef Medline
93. García-Mata, R., Wennerberg, K., Arthur, W. T., Noren, N. K., Ellerbroek, S. M., and Burridge, K. (2006) Analysis of activated GAPs and GEFs in cell lysates. *Methods Enzymol.* **406,** 425–437 CrossRef Medline
94. Pan, W., Borovac, J., Spicer, Z., Hoenderop, J. G., Bindels, R. J., Shull, G. E., Doschak, M. R., Cordat, E., and Alexander, R. T. (2012) The epithelial sodium/proton exchanger, NHE3, is necessary for renal and intestinal calcium (re)absorption. *Am. J. Physiol. Renal Physiol.* **302,** F943–F956 CrossRef Medline
95. Nagai, K., Yoshida, S., and Konishi, H. (2014) Gender differences in the gene expression profiles of glucose transporter GLUT class I and SGLT in mouse tissues. *Pharmazie* **69,** 856–859 Medline
96. Sotiropoulos, A., Gineitis, D., Copeland, J., and Treisman, R. (1999) Signal-regulated activation of serum response factor is mediated by changes in actin dynamics. *Cell* **98,** 159–169 CrossRef Medline